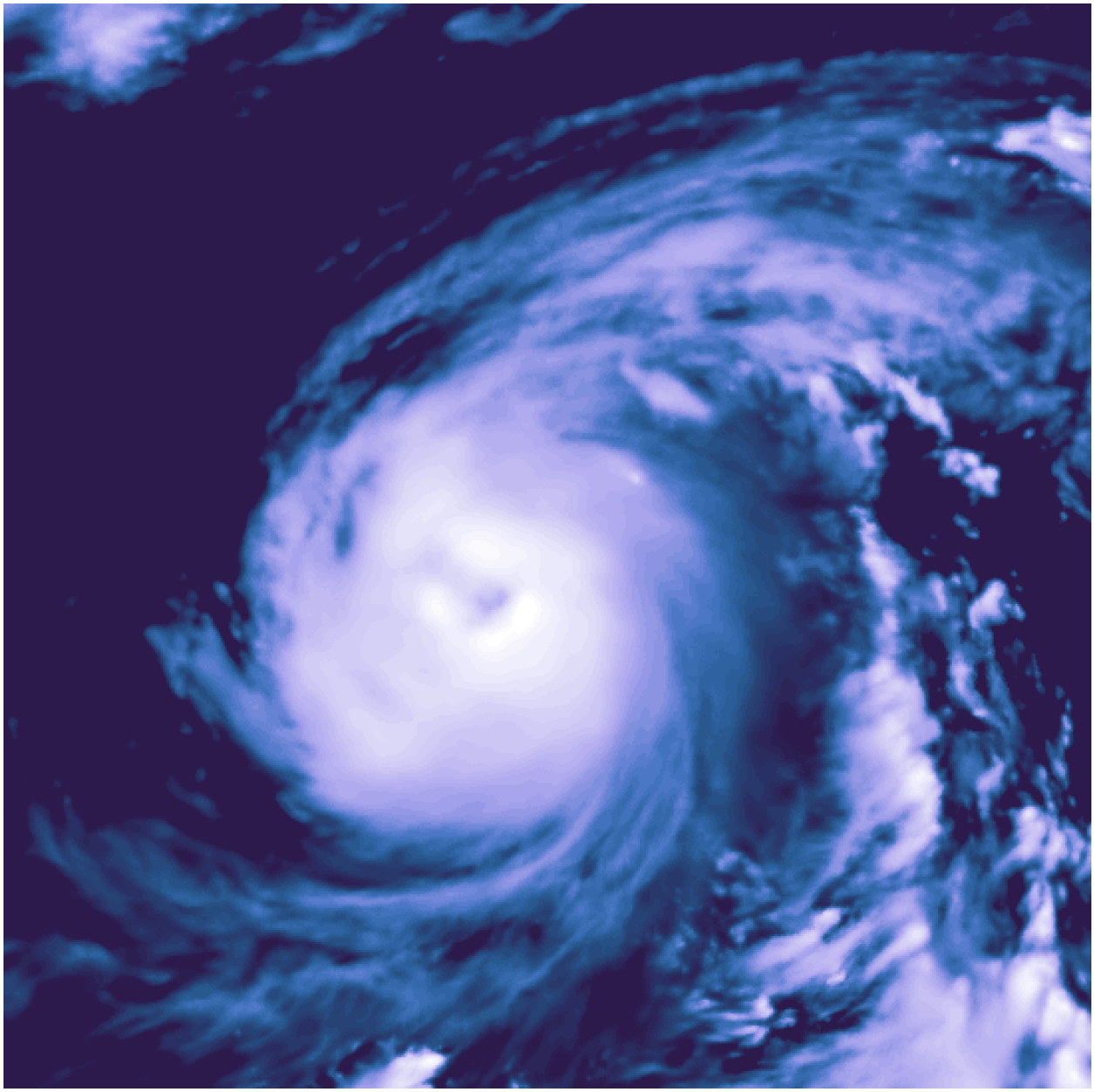

# The diurnal cycle of cloud ice water path

LARA LEKO

DEPARTMENT OF SPACE EARTH AND ENVIRONMENT

CHALMERS UNIVERSITY OF TECHNOLOGY
UNIVERSITY OF GOTHENBURG
Gothenburg, Sweden 2025
www.chalmers.se www.gu.se

Master's thesis 2025

# The diurnal cycle of cloud ice water path

A global diurnal analysis of ice water path as seen from Chalmers Cloud Ice Climatology

Lara Leko

UNIVERSITY OF GOTHENBURG

CHALMERS
UNIVERSITY OF TECHNOLOGY

Department of Space, Earth and Environment
*The Division of Geoscience and Remote Sensing*
Chalmers University of Technology
University of Gothenburg
Gothenburg, Sweden 2025

The diurnal cycle of cloud ice water path
A global diurnal analysis of ice water path as seen from the Chalmers Cloud Ice Climatology
Lara Leko



Supervisor: Patrick Eriksson, Department of Space, Earth and Environment
Examiner: Patrick Eriksson, Department of Space, Earth and Environment

Master's Thesis 2025
Department of Space, Earth and Environment
The Division of Geoscience and Remote Sensing
Chalmers University of Technology
University of Gothenburg
Gothenburg, Sweden 2025
www.chalmers.se
www.gu.se

Cover: Typhoon Megi on 27 September 2016, seen as total ice water path from the Chalmers Cloud Ice Climatology
Typeset in LaTeX
Gothenburg, Sweden 2025

The diurnal cycle of cloud ice water path
A global diurnal analysis of ice water path as seen from the Chalmers Cloud Ice Climatology
Lara Leko
Department of Space, Earth and Environment
Chalmers University of Technology

# Abstract

Ice clouds play a critical role in Earth's climate system through their impact on radiation and precipitation. Their diurnal variation, although vital for their net impact, remains poorly observed and simulated in models. This study presents the first global characterisation of the diurnal cycle of total ice water path (TIWP). This was done using the Chalmers Cloud Ice Climatology (CCIC), a novel satellite-derived dataset that combines CloudSat-based training with geostationary infrared observations.

Diurnal patterns in CCIC are compared with those from ERA5 reanalysis and GCRMs (Global Storm-Resolving Models) from DYAMOND project (DYnamics of the Atmospheric general circulation Modeled On Non-hydrostatic Domains). Results show that CCIC captures regional diurnal cycle contrasts: a strong diurnal cycle over land with an afternoon peak and a weaker diurnal cycle over oceans. ERA5 shows a dampened diurnal cycle with shifted peak times. The DYAMOND models offer an improved diurnal cycle representation.

These findings show that CCIC can be used as a tool for validating model representation of cloud processes. Validation at the diurnal level remains an important metric for model performance, both for reanalyses and emerging global models.

Keywords: diurnal cycle, clouds, cloud ice, climate models, remote sensing

# Acknowledgements

First and foremost, I would like to thank my supervisor Patrick Eriksson, for guiding me through this thesis. Without his systematic approach, knowledge and immeasurable patience, this work would not have been possible. I would also like to thank Adrià Amell Tosas, Peter McEvoy, Eleanor May and Anqi Li for for the discussions during our advisory meetings, for the patient technical support and for their kindness.

Lara Leko, Gothenburg, June 2025

# List of Acronyms

Below is the list of acronyms that have been used throughout this thesis listed in alphabetical order:

| | |
|---|---|
| CCIC | Chalmers Cloud Ice Climatology |
| CMIP | Coupled Model Intercomparison Project |
| CPMs | Covection-permitting models |
| DJF | December-January-February |
| DYAMOND | DYnamics of the Atmospheric general circulation Modeled On Non-hydrostatic Domains |
| ERA5 | The fifth generation ECMWF reanalysis for the global climate and weather |
| GSRM | Global storm-esolving models |
| ITCZ | Intertropical Convergence Zone |
| JJA | June-July-August |
| LST | Local Solar Time |
| LWCF | Long Wave Cloud Forcing |
| MAM | March-April-May |
| NH | Northern Hemisphere |
| SOM | September-October-November |
| SPCZ | South Pacific convergence zone |
| TIWP | Total Ice Water Path |

# Contents

# 1

# Introduction

Ice clouds play a crucial role in the Earth's climate system by significantly shaping the planet's radiation budget and influencing precipitation processes (Waliser et al., 2009). They reflect incoming solar radiation and alter the planetary albedo, effectively cooling the planet. At the same time, they absorb and re-emit thermal infrared radiation emitted from below them. Because of their high altitudes, clouds that contain ice, such as cirrus clouds and deep convective clouds, emit longwave radiation at lower temperatures and thus have the largest greenhouse effect (Lohmann et al., 2016). Whether the total effect of ice clouds on the climate will be a cooling or a warming one depends, among other factors, on their diurnal cycle. In deep convective clouds, their albedo effect prevails during the day. During the night, however, the greenhouse effect is more dominant. Since ice clouds are described as the most significant emitter of Earth's long-wave radiation (Duncan and Eriksson, 2018), any uncertainty about their properties, including their diurnal variation will have an impact on the global energy balance estimates.

In addition to their radiative effect, ice clouds, anvil and mixed-phase clouds in particular, are closely connected to the water cycle (Gong et al., 2018). The formation of ice releases latent heat, which drives the formation and development of convective storms (Bony et al., 2015). Ice particles are instrumental in the formation of precipitation. In the tropics, precipitation via the ice phase accounts for 69% of the total precipitation (Lau and Wu, 2003), and even more so in the higher latitudes. The diurnal timing of precipitation can influence surface evaporation and soil moisture Lai et al., 2025.

There is another reason to study the diurnal cycles of cloud ice. Seasonal and diurnal cycles are the two key variabilities in the Earth's weather and climate system, modulated by the changes in solar heating at the Earth's surface (Gong et al., 2018). However, the diurnal cycle is more poorly represented in climate models compared to the seasonal cycle, as it involves a wider range of processes and feedback mechanisms. Disagreements in the diurnal cycle often suggest misrepresentations of fundamental physical processes within models, even if longer-term averages show better agreement with observations (Christopoulos and Schneider, 2021). Consequently, the diurnal cycle is a crucial performance metric for climate models.

A common way to quantify ice in the clouds is its ice water path (IWP). This is a vertical integral of cloud mass through a column of the atmosphere. Both in global models and satellite observations, this variable varies to a large extent

(Duncan and Eriksson, 2018). This has at least partially been attributed to a vague definition of IWP (Waliser et al., 2009), which included ice particles suspended in the atmosphere. The term that combines all ice, both suspended and precipitating, is the total ice water path (TIWP). This is the sum of the mass of cloud ice, snow and graupel.

## 1.1 Diurnal measurements of cloud ice

Various satellite missions had the aim to quantify cloud ice. Among the validated cloud datasets we currently have available, CloudSat (Stephens et al., 2002) and CALIOP (Winker et al., 2010) are considered the most accurate. They have the ability to resolve the vertical structure of clouds and operate with a combination of active measurements at microwave, IR, and visible wavelengths. However, they are on a sun-synchronous orbit, meaning they measure any given spot on Earth at fixed local times. This makes them unsuitable for a diurnal cycle analysis. Moreover, CloudSat was decommissioned in 2023 and its role will be taken on by the EarthCARE mission (Illingworth et al., 2015. While data from different orbits can be combined to obtain some sampling of the diurnal cycles (Eriksson et al., 2010), these sensors can bring different systematic errors. SMILES (Superconducting Submillimeter-Wave Limb-Emission Sounder) flew on the International Space Station (ISS) in a non-sun-synchronous orbit, which means its observations weren't made at fixed local times. Over several months, it managed to provide a 24 h coverage(Kikuchi et al., 2010). More importantly, this instrument focused on the upper troposphere only and not on the total column. Geostationary satellites are most suitable for studies of diurnal cycles. However, their IR sensors provide only an indirect estimate of the cloud ice. They primarily observe cloud top temperatures, and provide little or no information on the interior of the cloud structure (Amell et al., 2024). The strongest diurnal cycles are found in regions covered with dense cloud decks. Here, microwave sensors would be needed to penetrate them. In short, no record has been able to provide a global TIWP estimate suitable for a diurnal analysis.

The Chalmers Cloud Ice Climatology (CCIC) is a new dataset that bridges the gap between sparse active sensor records and frequent but less informative IR data. It was trained on CloudSat using machine-learning, with continuous geostationary IR observations as input. CCIC provides near-global coverage of ice clouds at a temporal and spatial resolution high enough to investigate the diurnal cycle of TIWP for the first time. Anther important aspect is that CCIC can be used to compare to climate models. CCIC is further explained in Section 2.1. It will be used as a reference dataset in this thesis.

## 1.2 Climate models

General circulation models (GCMs) are mathematical models that represent physical processes of the atmosphere and ocean (Intergovernmental Panel on Climate

Change (IPCC), 2023). These models are widely used in climate studies, such as those participating in the Coupled Model Intercomparison Project phases 5 and 6 (CMIP5/CMIP6). Typical General Circulation Models (GCMs) have a horizontal resolution of 40 to 80 km. This means they are not capable of explicitly simulating the vertical energy transfer, which then determines deep convection, a mechanism at a scale of a few kilometres. Instead of explicit simulation, convection parametrization was used. A parameterization is a mathematical expression that describes the effect of a physical process on a subgrid scale, using a set of parameters derived from observations, theory, or higher-resolution models (Stensrud, 2007). Waliser et al. (2009) reported a factor of 20 difference between the largest and smallest values of ice water path in the GCMs they analysed. This was partly attributed to the vague definition of cloud ice and partly due to poorly resolved dynamic processes. In regards to their diurnal cycle representation, these models show persistent biases. Eriksson et al., 2014 observed the diurnal cycle of upper tropospheric cloud ice in three GCMs and revealed some problems in diurnal cycle estimation. These models have also shown persistent biases in simulating the diurnal cycle of precipitation, especially over land (Christopoulos and Schneider, 2021), with atmospheric convection parameterisation often considered the main reason (Song et al., 2024).

On the other hand, global storm-resolving models (GSRMs) have the spatial resolution of a few kilometers, which enables them to resolve these key convective processes explicitly. They also have a more direct physical representation of cloud microphysics. In many of these models the mass of all frozen hydrometeors in included in the output. They hold a potention for better cloud ice representation. The DYAMOND project (DYnamics of the Atmospheric general circulation Modelled On Non-hydrostatic Domains) is an initiative focused on intercomparing simulations from global storm-resolving models (GSRMs)(Stevens et al., 2019). The temporal resolution of GSRMs available in the DYAMOND dataset makes it possible for them to be evaluated at the diurnal level, which is, as previously mentioned, an important metric for climate models.

## 1.3 The diurnal cycle of upper-tropospheric cloud ice

Previous studies have found that the ice water content in the tropical upper troposphere shows an afternoon peak over land and an early morning maximum over the ocean. The strongest variations are observed in tropical land areas, with significant differences in amplitude and phase across regions, though these studies were limited by scarce measurements and focused only on the upper troposphere, as opposed to the whole cloud column (Eriksson et al., 2010; Eriksson et al., 2014; Millán et al., 2013; Jiang et al., 2015). Moreover, seasonal variability could not be taken into account as samples were taken during different months (Eriksson et al., 2014). The change in polarimetric difference (PD), determined by the microphysical properties of ice clouds, was found to lead the diurnal changes of their occurring frequency and total ice mass by about 2 h (Gong et al., 2018). More generally, the variations in ice

mass have shown a low degree of agreement across the data sets between different observational datasets and reanalysis (Duncan and Eriksson, 2018). With current observations, it has not been possible to derive the diurnal variation of TIWP for the entire column in the atmosphere.

## 1.4 Objectives

This study aims to create the first semi-global diurnal analysis of TIWP. The first objective is to describe the global and regional characteristics of the TIWP diurnal cycle as seen from CCIC. We will try to answer whether there are significant geographical or seasonal variations in the timing and strength of the peak TIWP. The second objective is to validate the TIWP diurnal cycle representation in ERA5 and GSRMs using CCIC as a reference.

# 2

# Data

## 2.1 CCIC CPCIR

The Chalmers Cloud Ice Climatology (CCIC) is a new dataset created to provide a continuous, long-term climate record of TIWP at a high resolution, addressing the limits of current observations. It's based on a machine learning model which connecting the patterns in the continuous IR observations, from the "true" ice mass from CloudSAT, specifically one of its retrieval products called 2C-ICE. The dataset covers the period from 2000 to the present, both during day and night, at a temporal resolution of 30 minutes and a spatial resolution of 0.036° (though with some gaps in spatial coverage in the early years). Measurements are limited to latitudes within 60° S to 60° N.

These retrievals were made from single-channel infrared (IR) observation, centred around 11 µm. Although they only provide information on the top of the cloud, they had the best spatial and temporal availability among the available gridded geostationary observations. The CCIC data records consist of two separate subrecords, which used two different observational data sets as input. These are CCIC (GridSat) and CCIC (CPCIR). In this thesis only CCIC (CPCIR) subrecord will be used. CPCIR comes from the Climate Prediction Center's globally merged IR product version 1, created at the National Oceanic and Atmospheric Administration (NOAA) (Janowiak et al., 2017).

In addition to TIWP, CCIC estimated the vertically resolved concentration of ice hydrometeors, known as total ice water content (TIWC), 2D and 3D cloud masks and a 3D cloud classification. However, they will not be used in this thesis.

The CCIC retrieval is based on a convolutional neural network (CNN) that uses quantile regression to provide probabilistic estimates of TIWP. It has been shown that neural-network-based retrievals can be considerably more accurate than traditional retrieval methods (Amell et al., 2024). Training data for TIWP and TIWC come from CloudSat's 2C-ICE product, which integrates radar and lidar observations. The CNN was trained using data from 2006 to 2009, while data from 2010 were used for model evaluation. Validation against training data achieved correlations above 0.7. CCIC was also validated against two in-situ air-borne and one ground-based cloud-radar measurements. Biases with respect to in situ measurements were

generally within or close to 50% for both flight campaign series, similarly to its training dataset. CCIC retrievals were shown to reproduce the diurnal cycle of TIWP as measured by a ground-based radar, across different seasons, at a correlation of above 0.7.

However, the limitations and biases of the 2C-ICE dataset itself need to be remembered. For example, Pfreundschuh et al., 2025 reported that 2C-ICE and CCIC estimates are about 20 % higher than the estimates from DARDAR, also a retrieval from CloudSat. Moreover, CCIC was found to overestimate low TIWP values (below 1 $kgm^{-2}$), and underestimate hight TIWP values, when compared to 2C-ICE (Amell et al., 2024), which could have an impact on the diurnal cycle.

Pfreundschuh et al., 2025 compared CCIC with other long-term TIWP records such as the International Satellite Cloud Climatology Project (ISCCP), Pathfinder Atmospheres—Extended (PATMOS-x), and the Moderate Resolution Imaging Spectroradiometer (MODIS). They found that the global mean values of TIWP can differ by a factor of three across different assessed observational datasets. CCIC estimates (both CPCIR and GridSat versions assessed in the paper) exhibit the highest global TIWP but align most closely with the two CloudSat-based reference products, considered the best currently available estimates (Pfreundschuh et al., 2025). CCIC will be used as a reference dataset throughout the thesis, as it is the only thoroughly validated TIWP data record with coverage suitable for diurnal analysis. However, it is important to keep in mind its limitations and inherited biases.

## 2.2 ERA5

ERA5 as the fifth generation ECMWF atmospheric reanalysis (Hersbach et al., 2020). Reanalysis combines model data with observations, in a process called data assimilation, into a globally complete and consistent dataset using the laws of physics. ERA5 provides hourly estimates for a large number of atmospheric variables. The sum of two variables: the total column snow water (SIWP) and total column ice water (CIWP), will be used as a TIWP estimate. Pfreundschuh et al., 2025 note that this does not not represent all frozen hydrometeors, as graupel is not included. The estimation of SIWP and CIWP within ERA5 is a result of its underlying Integrated Forecasting System (IFS) and its parametrisation schemes (Dou et al., 2020).

Globally, Duncan and Eriksson, 2018 found that ERA5 provides TIWP estimates that differ significantly in magnitude compared to other available TIWP records. Compared to CloudSat/CALIPSO-based reference measurements (2C-ICE and DARDAR), which are considered the most accurate cloud ice estimates, it was shown to underestimate higher TIWP values, especially in the tropics (Pfreundschuh et al., 2025). There was still good agreement regarding key climate features and seasonal variability.

ERA5 is not an observational dataset, and it's hydrometeor distribution is determined by its parametrisation schemes, which can induce uncertainties (Pfreundschuh

et al., 2025). The ability of ERA5 to reproduce the diurnal cycle thus needs to be validated. Dai, 2024 studied the diurnal cycle of ERA5 for various meteorological fields and compared it to observations. ERA5 mostly reproduced the observed land-ocean contrast in the diurnal cycle of warm-season precipitation, with a peak over land in the afternoon and over oceans in the early morning. However, it had a tendency to peak slightly earlier. Additionaly, it captured net shortwave and longwave radiation diurnal cycles and their land–ocean and seasonal differences.

## 2.3 DYAMOND

The DYAMOND project (DYnamics of the Atmospheric general circulation Modeled On Non-hydrostatic Domains) is the first global high-resolution simulation intercomparison, where the storm-resolving simulations are performing the same experiment. Two experiment phases have been implemented so far, the one covering boreal summer and the one covering austral summer. The second phase (DYAMOND Winter) included coupled atmosphere-ocean simulations, starting from 20th January 2020 and integrated for 40 days. This phase involved twelve models with a minumum grid spacing of 5 km. The models were initialised using the same European Center for Medium Range Forecasting (ECMWF) atmospheric analysis and were run with prescribed sea surface temperatures from a 7-day running mean. Soil moisture was initialised using best practices for each model. Nine models were used for this study. The requirement was that they included cloud ice, snow and graupel in their estimate of TIWP. Only IFS contained no graupel in the output. Still, it was included in the report due to it's relevance.

The models vary in their grid structure, microphysics, parameterisations for unresolved processes (like shallow convection and boundary layer), and how they handle ice species. All models are non-hydrostatic, again with IFS as an exception. The term "non-hydrostatic" in atmospheric modelling generally means that the model's equations do not assume hydrostatic balance in the vertical direction. This assumption is valid for large-scale motions but breaks down for smaller-scale phenomena like convection, where vertical accelerations are significant. Non-hydrostatic models include the vertical acceleration terms, making them suitable for explicitly resolving these motions (Wedi and Malardel, 2010).

Where possible, models that use ocean coupling (OC) are included. Ocean coupling refers to the interaction between the atmosphere and the ocean, where they exchange energy, momentum and mass. Changes in the sea surface temperature (SST) induce changes in heating or cooling of the atmosphere, which alters atmospheric circulation, winds and heat fluxes at the ocean surface (Fedorov, 2007). The models, their resolution, type of convection parametrisation and whether they used ocean coupling are included in Table 2.1.

Further details on the DYAMOND simulations are shown in Stevens et al., 2019. DYAMOND data management was provided by the German Climate Computing Center (DKRZ), where it was standardized to simplify their analysis and ease com-

parisons, and supported through the projects ESiWACE and ESiWACE2, which have received funding from the European Union's Horizon 2020 research and innovation programme under grant agreements No 675191 and 823988. The DYAMOND data sets were accessible via the The DYAMOND Data Library, which is situated at DKRZ's supercomputer Levante. The data used in this thesis was previously processed by Nils Müller. As projects utilised different grid structures, this included remapping the model data to a common 0.1° lon-lat grid. This was done using the conservative remapping function from Climate Data Operators (CDO) (Schulzweida, 2023). Additional fixes were done to homogenise the data.

| **Model** | **Resolution (km)** | **Resolution (min)** | **CP** | **OC** |
|---|---|---|---|---|
| GEM | ∼5 | 60 | None | No |
| GEOS | ∼3 | 15 | Full | No |
| GFDL | ∼3 | 15 | Shallow | No |
| GRIST | ∼5 | 15 | None | Yes |
| GSAM | ∼4 | 15 | None | No |
| ICON | ∼5 | 15 | None | Yes |
| IFS | ∼4 | 60 | Shallow | Yes |
| MPAS | ∼3.75 | 15 | Full | No |
| ARPEGE | ∼2 | 15 | None | No |

**Table 2.1:** DYAMOND models, their spatial and temporal resolution, Convective Parametrisation (CP) and Ocean Coupling (OC).

DYAMOND simulations have been used for intercomparing cloud properties, such as outgoing longwave radiation (OLR), net shortwave radiation (NSR), and the vertical structure of cloud water, cloud ice, and cloud fraction. These intercomparisons revealed large variations across models in vertical structure, though all models reproduced the expected triple peaks corresponding to shallow, congestus, and deep clouds (Roh et al., 2021). Song et al., 2024 used the project dataset to evaluate the precipitation diurnal cycle, showing that DYAMOND CPMs have an improved capability in reproducing the observed timing and amplitude compared to CMIP6 high-resolution and low-resolution models. The improved performance in CPMs was linked to their ability to better simulate mesoscale convective systems (MCSs), their lifecycle and the timing of their mature stage (when high clouds and associated ice mass shoul to be the highest). Hence, they are expected to produce a more realistic diurnal cycle for the high clouds and IWP associated with these systems.

# 3

# Methods

## 3.1 Conversion to local solar time

The time conversion from UTC to local solar time (LST) was done for each grid cell using this equation, assuming $lon \in [-180, 180]$:

$$LST = UTC + \frac{lon}{15° h^{-1}}. \tag{3.1}$$

## 3.2 Fitting of the diurnal cycle

Two characteristics that can be used to describe the diurnal cycle are its amplitude and its peak time. The diurnal cycle can be largely described with a periodic curve, a sinusoid with a 24-hour period and another one with a 12-hour period. Additional components were not found to provide additional value (Watters and Battaglia, 2019). The diurnal cycle of TIWP was determined in each grid box by conducting a harmonic analysis. A least squares method was used to fit the half-hourly TIWP estimates using the harmonic function F(t) defined by:

$$F(t) = M_0 + S_1 \sin(\frac{2\pi t}{24}) + C_1 \cos(\frac{2\pi t}{24}) + S_2 \sin(\frac{2\pi t}{12}) + C_2 \cos(\frac{2\pi t}{12}). \tag{3.2}$$

where t is the time of day, $M_0$ is the mean, $S_1$ and $C_1$ are the diurnal coefficients and $S_2$ and $C_2$ are the semi-diurnal coefficients.

The amplitude of the diurnal cycle $A$, is defined as the distance between the daily minimum and the daily maximum after the fit, whereas peak time $t_{\text{peak}}$ is the time when the function reaches the maximum:

$$A = F(t)_{max} - F(t)_{min}, \tag{3.3}$$

$$t_{\text{peak}} = \underset{t \in [0,24)}{\arg\max}\ F(t). \tag{3.4}$$

Examples can be found in Appendix A.1. This model will be used in the global

analysis of amplitude and peak time. The diurnal ($t_{\text{peak},24}$) and semi-diurnal ($t_{\text{peak},12}$) components to the fit will also be analysed separately, in order to identify their contributions to the fit. The amplitudes $A_1$ and $A_2$ can be defined analytically as:

$$A_1 = 2\sqrt{S_1^2 + C_1^2}, \tag{3.5}$$

$$A_2 = 2\sqrt{S_2^2 + C_2^2}. \tag{3.6}$$

Their respective peak times are ($t_{\text{peak},24}$) and ($t_{\text{peak},12}$). For the semi-diurnal component which peaks twice daily, there is another peak time, 12 hours later than defined here:

$$t_{\text{peak},24} = \left(6 - \frac{12}{\pi} \arctan 2(S_1, C_1)\right) \bmod 24, \tag{3.7}$$

$$t_{\text{peak},12} = \left(3 - \frac{6}{\pi} \arctan 2(S_2, C_2)\right) \bmod 12. \tag{3.8}$$

The 'goodness of fit' of the modelled diurnal variation in Eq. (3.2) compared to the original diurnal cycle is described with explained variance ($R^2$) (Jeong et al., 2011). Explained variance describes how much of the total variance in the data is explained by the fitted function.

The explained variance is defined by:

$$R^2 = 1 - \frac{\text{RSS}}{\text{TSS}}. \tag{3.9}$$

Here, the residual sum of squares (RSS) and the total sum of squares (TSS), are defined as:

$$\text{RSS} = \sum_{i=1}^{n} (y_i - \hat{y}_i)^2, \tag{3.10}$$

$$\text{TSS} = \sum_{i=1}^{n} (y_i - \bar{y})^2, \tag{3.11}$$

where $y_i$ are the observed data values, $\hat{y}_i$ the fitted values, and $\bar{y}$ the mean of the observed data.

A value of $R^2$ close to 1 indicates that the model explains most of the variance in the data.

# 4

# Results & Discussion

The diurnal cycle of TIWP as seen from the CCIC (Chalmers Ice Cloud Climatology) record is described in section 4.1. Section 4.2 compares the global mean and the diurnal variations to ERA5, the global ECMWF atmospheric reanalysis. Section 4.3 builds on these results to evaluate the diurnal representation of TIWP in DYAMOND climate models.

## 4.1 The diurnal cycle in CCIC

The diurnal cycle in CCIC was determined using six years of TIWP data, from 2018 to 2023. Although, a longer analysis (e.g., at least 20 years) is usually needed to exclude the influence of interannual variability and describe the climatology, this was not done due to some missing data in the earlier years. Nevertheless, during this period, neither of the two phases in the ENSO (El Niño-Southern Oscillation) cycle was favoured. The diurnal cycle of precipitation was previously found not strongly impacted by El Nino events (Watters and Battaglia, 2019). More importantly, inluding the earlier years could also introduce the effect of climate change.

The global distribution of mean TIWP is shown in Fig. 4.1, for the four seasons, regridded to a 1° grid cell. The highest TIWP values are closely related to zones of tropical deep convection. Parts of the Amazon and central Africa, and the Maritime Continent (Indonesia, Papua New Guinea, surrounding seas) and the Intertropical Convergence Zone (ITCZ) stand out in particular. Higher TIWP values are also found in the warmer seasons, due to higher convective activity. TIWP minima are found over the subtropical regions of large-scale descent. In the mid-latitudes, regions associated with extratropical cyclones exhibit higher TIWP values, especially in the winter season. Influence of mountain ranges is visible in the Himalayas and the Andes. The global mean TIWP distribution was already reported in Pfreundschuh et al., 2025 and here serves for context. The abbreviations for the four seasons are DJF (December, January, February), MAM (March, April, May), JJA (June, July, August) and SON (September, October, November).

### 4.1.1 Mean regional diurnal cycles

These results will describe the mean diurnal cycle over six regions which represent different diurnal cycle regimes. These regions are shown in Fig. 4.2 and were taken

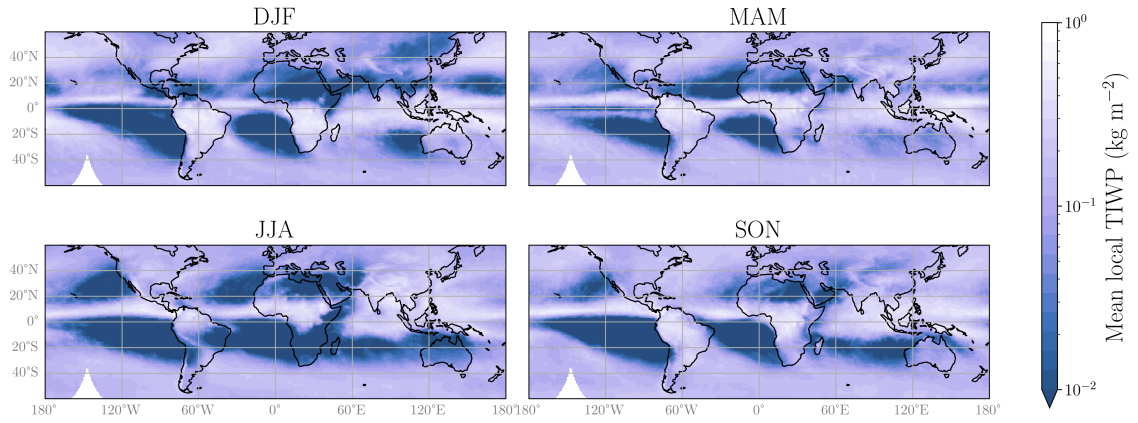


**Figure 4.1:** Mean local TIWP in CCIC for the period 2018 to 2023 at a 1° spatial resolution.

from Eriksson et al., 2014 to allow for comparison with the paper. To explore this diurnal cycle, for each month in the study period, an "average day" was computed at every 1° grid cell, binning the data into each 30-minute intervals and averaging. Fig. 4.3 shows mean diurnal cycles of TIWP averaged over these regions. Their respective relative diurnal cycles are also shown on the right side. The regions are defined in Fig. 4.2. Land regions (Africa, South America) show strong diurnal TIWP cycles peaking in the afternoon, consistent with solar-driven convection. TIWP during boreal winter in both regions peaks around 16:30, at around 0.60 $kgm^{-2}$ for Africa and 0.67 $kgm^{-2}$ for South America. These diurnal cycles closely resemble the ones reported by Eriksson et al., 2014, which used observations from SMILES (Superconducting Submillimeter-Wave Limb-Emission Sounder), an instrument on a non-sun-synchronous orbit. The values in the study focused on upper tropospheric ice, as opposed to the whole column ice, which can account for lower absolute amplitudes and later peak times than reported here. Moreover, since SMILES sampled different parts of the diurnal cycles during different months, seasonal impacts could not be separated. Outside of the tropics, higher TIWP is generally stronger in the warmer months, due to enhanced convection. CCIC was able to discern between seasons, showing that for these continental regions, amplitude did have a seasonal dependency, with the highest values in summer months.

Oceanic regions (Tropical Indian, Pacific areas) show weaker cycles, with flatter profiles and a weaker diurnal cycle, due to relatively weaker oceanic convection compared to land convection (Tian et al., 2004). The North Pacific area shows the overall lowest concentrations of TIWP, associated with the descent in the Hadley cell (Eriksson et al., 2010). The Tropical Indian region peaks around 04:00, and the Tropical Pacific region an hour later. This is consistent with Yang and Slingo, 2001, who showed that the deepest clouds are most prevalent in the early morning over tropical regions. Both regions also exhibit a secondary peak around 14:00. This cycle is driven by a different set of processes which are not as straightforward as over land. The peak time over the ocean coincides with the peak of large organised convection systems, which are infuenced by more varied processes. Johnson et al.,

1999 described three cloud modes over oceanic convective regions: 1) morning low cloud, 2) afternoon scattered convection, and 3) nocturnal organised convection.

The Maritime Continent acts as a transitional zone, combining land-sea effects and exhibiting bimodal behaviour, as was mentioned in Hong et al., 2006.

Overall, the TIWP diurnal cycle is more pronounced over land, with peaks in the afternoon, connected to surface temperature. This diurnal variation is linked to the diurnal variation of cloudiness, deep convection and humidity, with all these diurnal cycles associated with the 24 h variation of the solar forcing (Millán et al., 2013). Over the ocean, the signal is weaker and often peaks in the early morning, associated with organised convection.

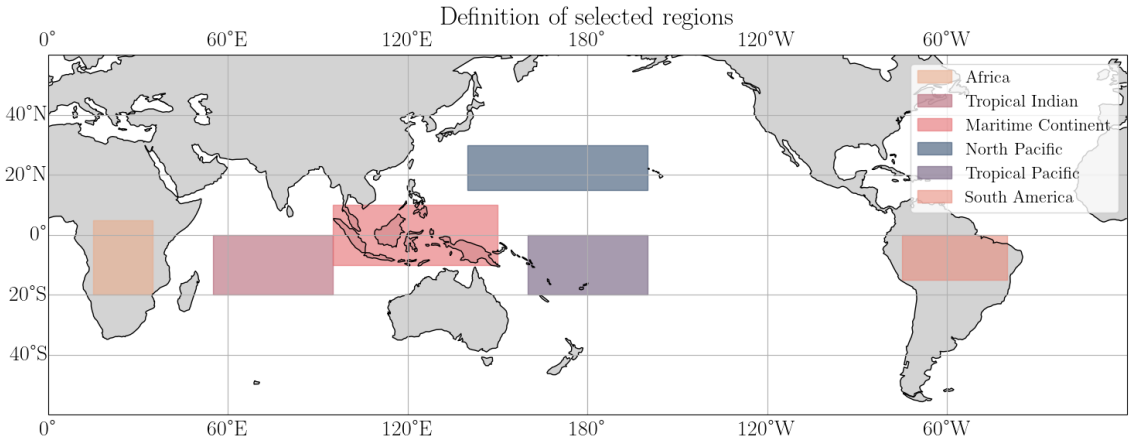


**Figure 4.2:** Definition of the selected regions.

### 4.1.2 Global diurnal amplitude and peak time

In the next part, the diurnal cycle in CCIC is analysed on a local level. Further spatial averaging to a 5° grid cell was necessary to obtain stable diurnal cycle signals. The diurnal cycle of TIWP can be subtle and often obscured by noise, particularly over oceanic regions. As was seen in the mean regional cycles, some regions also exhibited a semi-diurnal component. The mean diurnal curve was fitted with the diurnal (24 h, S1) and semidiurnal (12 h, S2) harmonics at each grid point to obtain the TIWP amplitude and peak time. The results are shown in Fig. 4.4.

As it was seen in the regional averages, land regions show stronger and more consistent afternoon peaks (15:00–19:00 LST) across all seasons and oceans display more scattered peak times with weaker amplitudes, generally clustering around 03:00–06:00 LST in the tropics. Extratropical ocean regions generally peak later, such as in SH (Southern Hemisphere) summer where TIWP peaks in late afternoon. There are, however large regional differences.

The highest amplitudes are strongly localised over continental tropical deep convective zones: the Congo and Amazon Basins, and the Maritime Continent. Convective regions at higher latitudes have an amplitude with a stronger seasonal de-

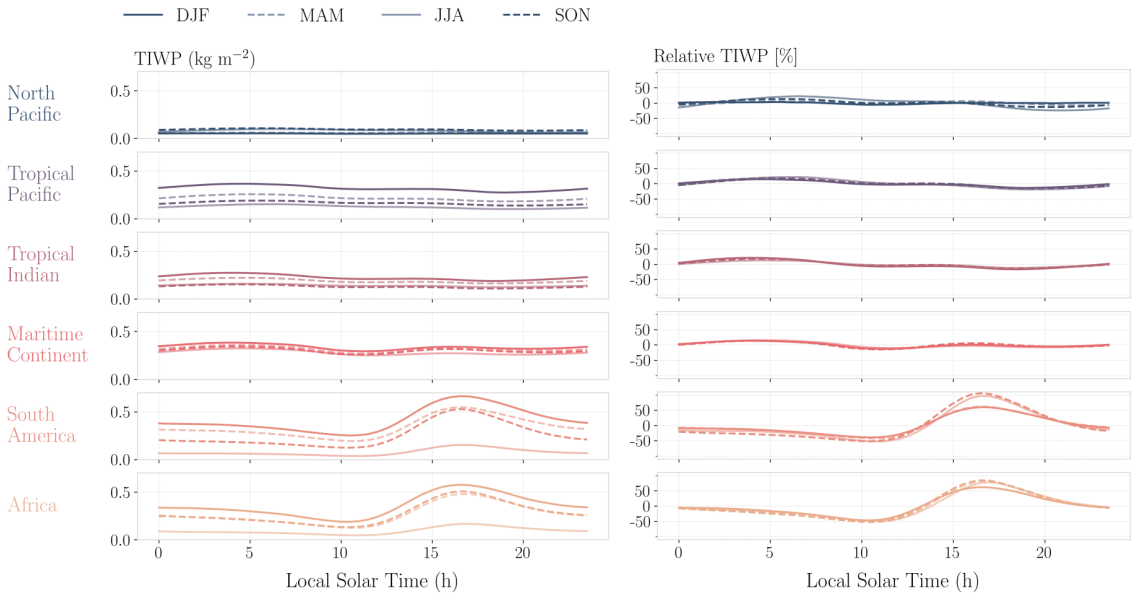


**Figure 4.3:** Mean diurnal cycles of TIWP in CCIC for selected regions from 2018 to 2023. Absolute TIWP is shown on the left and the relative deviation from the local mean on the right.

pendence. Higher amplitudes are also found in northern India and Southeast Asia during JJA, associated with the monsoon season. As monsoons move toward Australia in DJF, higher amplitudes are found there, and a more consistent afternoon peak time.

Infuence of orographic lifting can be seen on both amplitude and phase of the diurnal cycle. The Tibetan plateau shows consistently higher values of TIWP. This region is an important modulator of Asian climate, as surface heating creates a low-pressure center resulting in warm and moist air convergence from the ocean and enhanced convective activity (Zhao et al., 2023). These conditions allow for an afternoon convection peak over the TP (Tibetan Plateau). Over its east periphery, however, peak time is shifted to late evening and night hours.

Spread from land convective regions to the adjacent oceans, formerly observed in the diurnal cycle of precipitation (Yang and Slingo, 2001), suggests land-sea-breeze effects. This results in higher amplitudes and later peak times compared to adjacent ocean areas. This can be seen along the Central American and Mexican coasts in JJA and around the islands of the Maritime Continent.

Oceanic regions show weaker amplitudes overall, with some seasonal enhancement in the ITCZ and SPCZ. The peak time in these oceanic convective regions exhibits a range of values from early morning to evening with significant seasonality. Generally, oceans peak in the morning in tropical regions. However, around 30°S, oceanic TIWP has an afternoon peak in DJF, similar to land. Afternoon maxima in convective precipitation have previously been found over some oceanic areas such as the South Pacific Convergence Zone (SPCZ), the tropical central and eastern Pa-

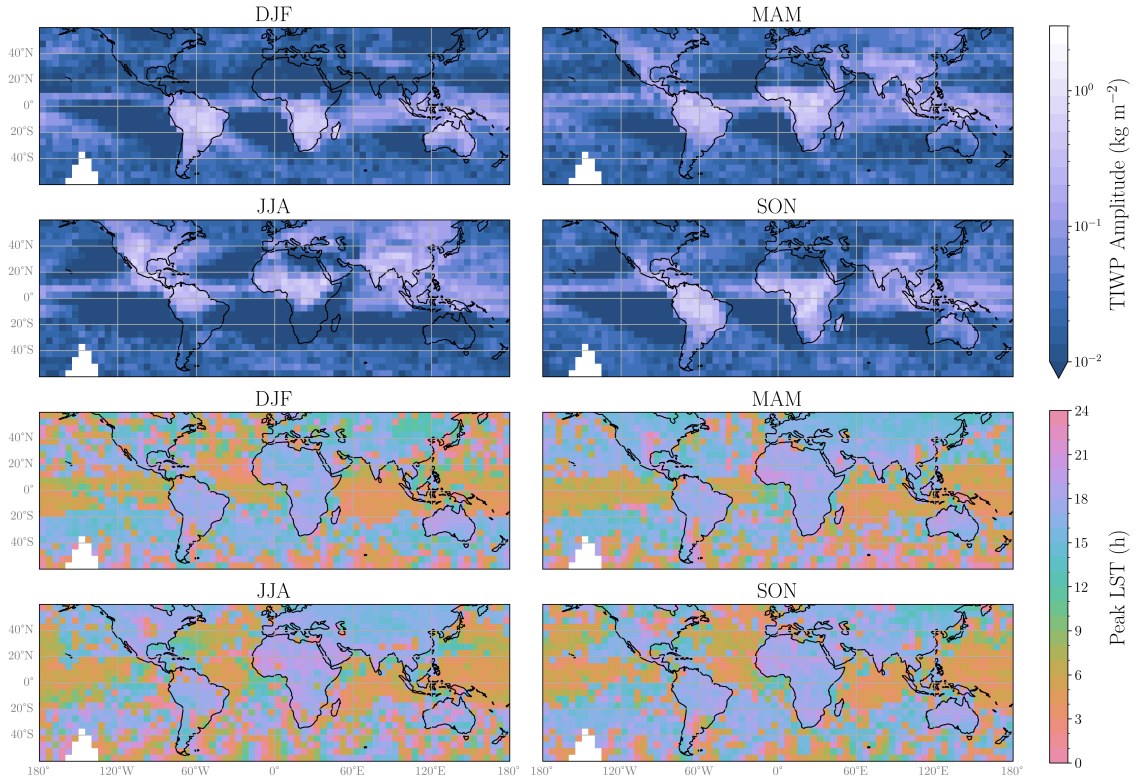


**Figure 4.4:** Diurnal amplitude (top) and peak time (bottom) after a harmonic fit, for the years 2018 to 2023 at a 5°x5° resolution. Amplitude is defined as the daily maximum minus the daily minimum. The results are shown for the four seasons separately.

cific (Dai, 2001). Sui et al., 1997 reported that only the deep, organised convection shows an early morning peak whereas submesoscale convection, in the large-scale subsidence regimes, shows a late afternoon maximum, similar to land-based convection. Outside of the tropics, oceanic regions show a much weaker diurnal cycle and an ambiguous peak time. This can be seen in Fig. 4.5, where the "goodness of fit" increases for tropical land and for the warm seasons.

Variance explained by the diurnal component shown in Fig. 4.6 shows that the 24-h mode is the primary driver of the TIWP cycle, compared to the semi-diurnal component shown in Fig. 4.7. This was observed previously in Dai, 2001 for showery summer precipitation and thunderstorms over land, where the diurnal cycle accounted for up to 80% of the daily variance as opposed to the semidiurnal cycle (around 15% - 25%). This is because the solar heating cycle is the primary mechanism of continental convective development. This cycle induces a diurnal cycle of opposite phase over large oceanic areas nearby that favours a morning maximum of maritime showery precipitation. The mechanisms over remote oceans are more complex and involve multiple interacting processes, but mostly with a diurnal period. Dai, 2001 suggests that over open oceans, the 12-h cycle is related to the semidiurnal atmospheric tide in the pressure field.

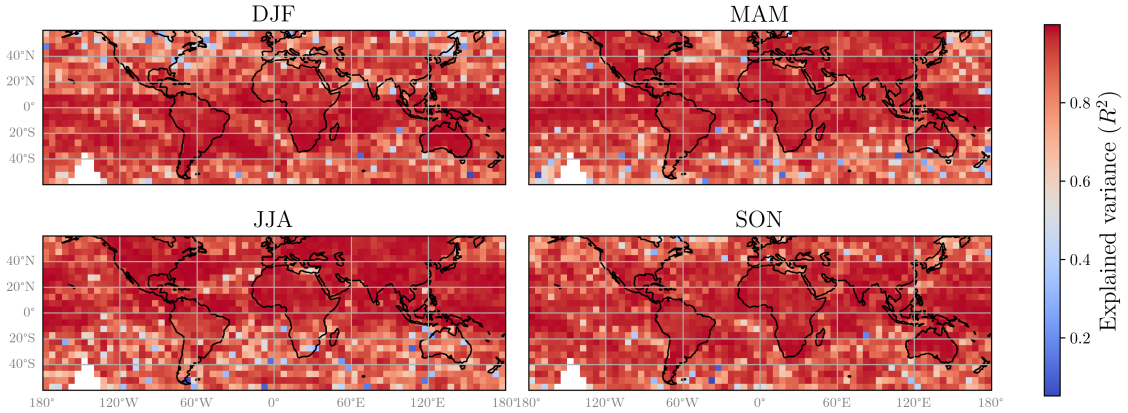


**Figure 4.5:** Explained variance ($R^2$) of the diurnal cycle by the full fit at each 5°x5° grid cell, for the years 2018 to 2023.

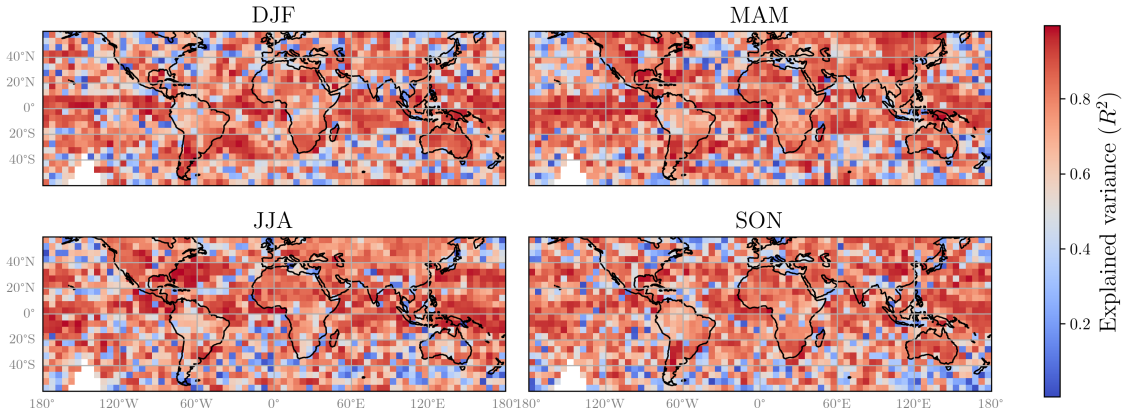


**Figure 4.6:** Explained variance ($R^2$) of the diurnal cycle by the 24-hour component at each 5°x5° grid cell, for the years 2018 to 2023.

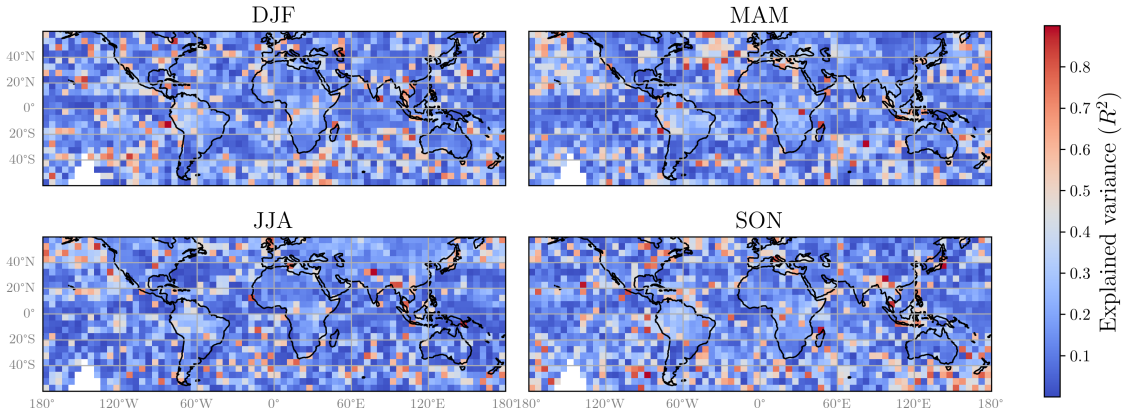


**Figure 4.7:** Explained variance ($R^2$) of the diurnal cycle by the 12-hour component at each 5°x5° grid cell, for the years 2018 to 2023.

## 4.2 The diurnal cycle in ERA5

In this section, CCIC is used as a reference for evaluating ERA5, the fifth generation ECMWF atmospheric reanalysis, introduced in section 2.2. The global distribution of mean TIWP in both CCIC and ERA5 is shown in Fig. 4.8. Both datasets show similar spatial distribution and seasonal variation, though ERA5 has visibly lower TIWP estimates. This was already reported in Pfreundschuh et al., 2025 where ERA5 underestimated global TIWP estimates both compared to both CCIC and the CloudSat/CALIPSO observations, due to the exclusion of graupel. The diurnal cyces of these datasets will be compared in relative terms.

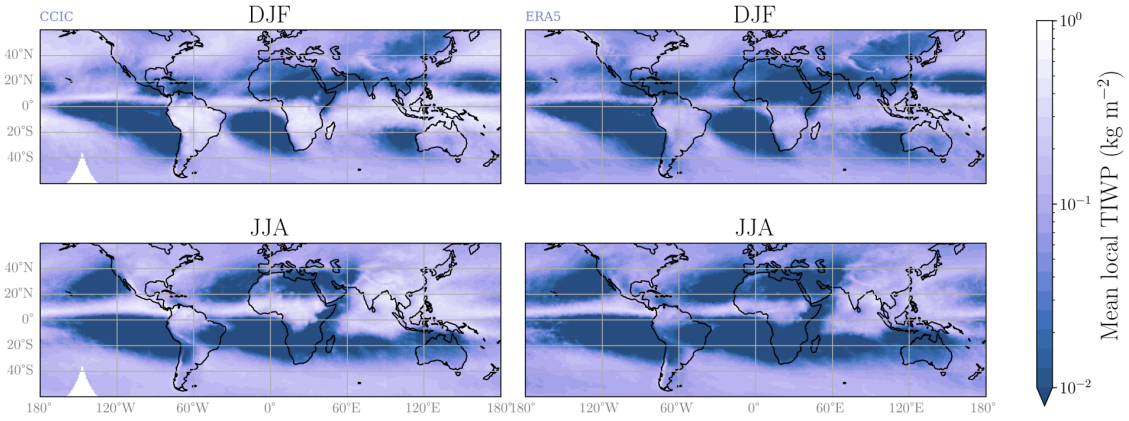


**Figure 4.8:** Mean local TIWP in CCIC (left) and ERA5 (right) for the period 2018 to 2023 at a 1° spatial resolution.

### 4.2.1 Mean regional diurnal cycles

Diurnal cycles of six regions in ERA5 were acquired in a similar way as in CCIC. Both are compared in Fig. 4.9 as relative deviation to the mean. Over land, strong diurnal signals with an afternoon peak are not found in ERA5. Over South America, relative TIWP in JJA peaks around noon and has a minimum in the afternoon. During DJF the diurnal cycle is less defined and peaks around midnight. While there is an afternoon peak over Africa, it is comparable to, and even surpassed by, an early morning peak. Unlike relative amplitudes in CCIC that reach 100%, in ERA5 they only reach 50%. The diurnal cycle over the ocean is even less defined, with the early morning peak found in CCIC over tropical oceans largely missed. Over the Maritime Continent the peak is found around noon, out of phase with CCIC.

ERA5 is not an observational dataset and the TIWP seen is a result of its parametrisation schemes, which can explain this performance. Additionaly, Dai, 2024 reported that ERA5 oceanic convective precipitation showed a dampened diurnal cycle due to its use of daily-mean sea surface temperature (SST) as a lower boundary condition. This means ERA5 does not include oceans heating up during the day and cooling during the night. Diurnal SST variations often accompany atmospheric SST variations. For example, large diurnal SST variations were observed

during convective event development over the tropical Indian Ocean in Bellenger et al., 2010. In Dai, 2024, the overall cycle characteristics of convective precipitation were comparable to observations. Here, in the case of TIWP, ERA5 doesn't seem to capture the phase or the amplitude of the diurnal signal.

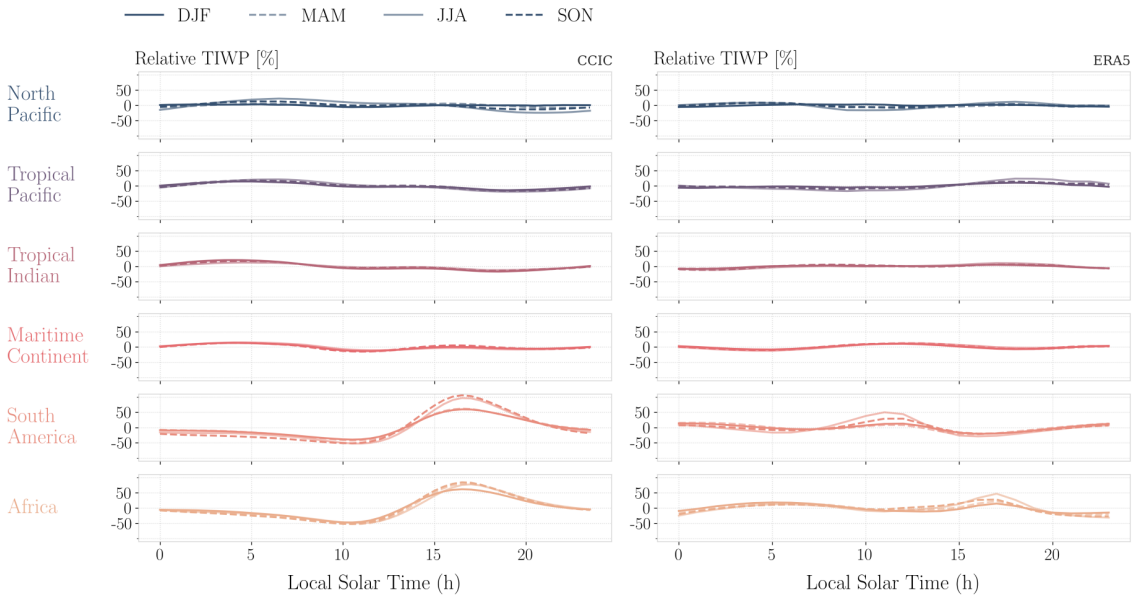


**Figure 4.9:** Deviation from mean TIWP [%] in CCIC (left) and ERA5 (right) for selected regions from 2018 to 2023.

### 4.2.2 Global diurnal amplitude and peak time

Harmonic fitting at each 5 ° grid cell and the resulting amplitude and peak time for ERA5 was carried out in the same way as for CCIC. Since DJF and JJA months captured most of the seasonal variations, only they were included in the comparison. Results are shown in Fig. 4.10. All four seasons can be found in the Appendix A.2. Amplitude of the diurnal cycles in regions of tropical deep convection are visibly underestimated in ERA5, even in relative terms. Over central Africa and South America, peak time is shifted to early morning hours. While CCIC exhibits an early morning peak over large parts of the tropical ocean, in ERA5, this is not as clear. The afternoon peak in SH extratropical oceans observed in CCIC can also be seen in ERA5. There are some differences in the central Pacific Ocean and Indian Ocean. Interestingly, for convective precipitation, an afternoon extratropical peak was not observed in convective ERA5 (Dai, 2024). As with CCIC, the diurnal variation in ERA5 is largely explained by the diurnal mode which is shown in Fig. 4.11. The diurnal component was previously shown to dominate the diurnal variations in precipitation, cloud cover and other ERA5 variables (Dai, 2024), while semidiurnal component's contribution was to improve the fit. Interestingly, the semi-diurnal component over the Maritime Continent region here dominates. Both are included in the Appendix A.2 for four seasons, where the explained variance of the full fit is also found.

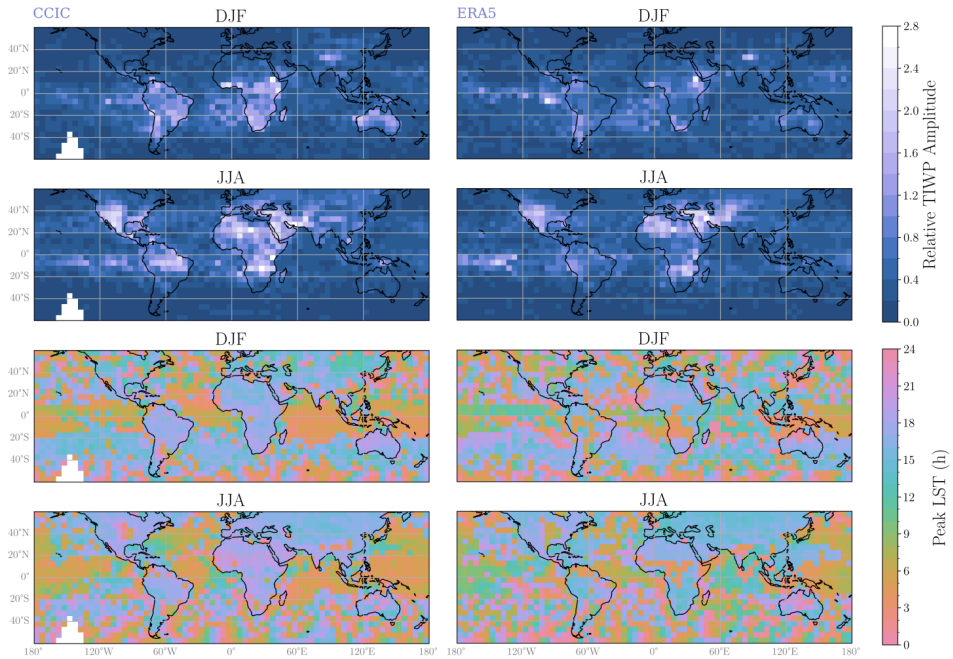


**Figure 4.10:** Diurnal amplitude (top) and peak time (bottom) after a harmonic fit, for the years 2018 to 2023 at a 5°x5° resolution, for CCIC (left) and ERA5 (right) in summer and winter seasons.

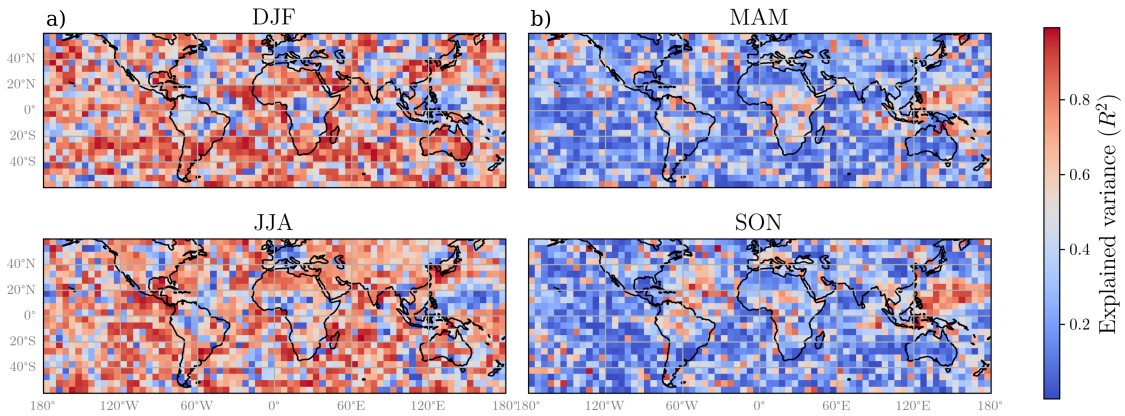


**Figure 4.11:** ERA5 explained variance ($R^2$) of the diurnal cycle by the 24-hour component (a) and 12-hour component (b) at each 5°x5° grid cell, for the years 2018 to 2023.

## 4.3 The diurnal cycle in DYAMOND

In this section, the CCIC record is compared to model outputs from the DYAMOND project. This included nine global storm-resolving models, which estimated TIWP, described in section 2.3. Local means of TIWP for DYAMOND (average from all nine modeles) and CCIC are shown in Fig.4.12 for February 2020. Overall, the global distribution of the DYAMOND average and CCIC look very similar. Compared to CCIC, DYAMOND underestimates the highest TIWP values found in the tropical regions: South America, central Africa, the Indian Ocean, ITCZ and SPCZ. Storm tracks in the Atlantic, where extratropical cyclones were shown to grow, forced by the Gulf Stream (Businger et al., 2005) also show higher TIWP values in CCIC. Except for these high values, the spatial distribution of TIWP is generally well reproduced in the models, following the same shape of the ITCZ and the subtropical regions of subsidence. Orographic features are clearly visible in both. Notice that CCIC could have a bias towards higher values, as discussed in section 2.1.

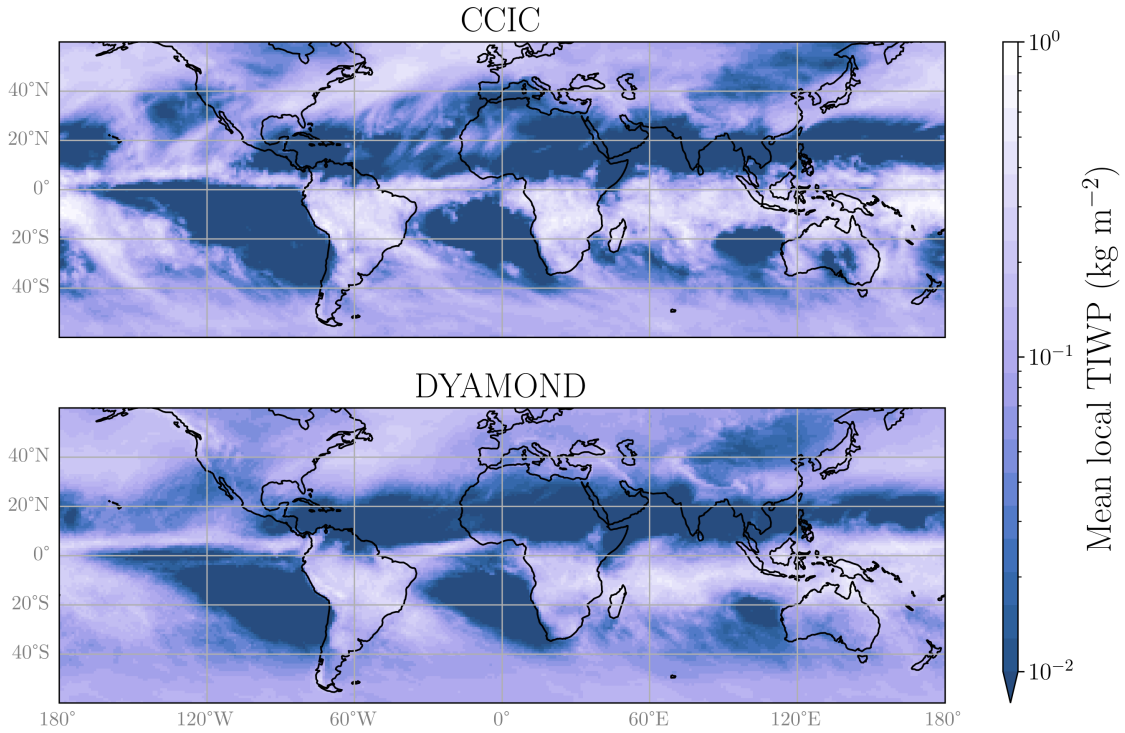


**Figure 4.12:** Local mean TIWP in CCIC (top) and DYAMOND average (bottom) for February 2020 at a 1° spatial resolution.

### 4.3.1 Mean regional diurnal cycles

Here the diurnal cycles for the six regions defined in section 4.1.1 are shown for the DYAMOND models. These are the GSRMs that have a spatial resolution sufficient to represent convection explicitly. Compared with with CCIC, their mean regional diurnal cycles are shown in Fig. 4.13. Regional diurnal means were acquired in the same way as for ERA5 and CCIC. The diurnal cycle is also shown in relative

terms in Fig. 4.14. Over tropical land, most models manage to reproduce the diurnal cycle with an afternoon peak, typical for land regions. The GEM model is an obvious exception, where pronounced diurnal cycles are not seen. In absolute terms, CCIC generally shows higher values of TIWP compared to the DYAMOND models. Only IFS and GEOS show comparably high values. However, as noted before, CCIC estimates could be on the higher side. Over ocean regions, IFS even surpasses CCIC. GEOS shows large differences in absolute value from land to ocean areas. CCIC peaked between 16:30 and 17:00 in tropical land. Most models peaked earlier than CCIC, from 14:00 to 16:00, which is reflected in the DYAMOND average (Fig. 4.14), suggesting that models initialise convection earlier. The IFS peak time best coincides with the peak time of CCIC. While GEOS has a pronounced diurnal cycle, it tends to peak too early. For example, it peaks more than two hours earlier over Africa. In relative temrs, ARPEGE also resembles CCIC very well. A clear land diurnal cycle is visible in GRIST, ICON, GFDL and MPAS. The diurnal cycle of GSAM over South America is not pronounced and peaks too early over Africa. The TIWP minimum, which in CCIC occurs around 11:00, also occurred slightly earlier in most models. Song et al., 2024 already reported 2 h earlier peak times for DYAMOND models over land, although for precipitation from Mesoscale Convective Systems, an important source of precipitation in the tropics. There too, IFS best matched with the peak in observations. However, this was a major improvement compared to GCMs, which peaked 4-5 h earlier compared to observations.

Over the tropical ocean, a weaker diurnal cycle with a primary peak in the morning and a secondary peak in the afternoon is mostly captured in DYAMOND models. The secondary peak around 14:00 is sometimes visible. Overall, the diurnal cycle over the ocean is not as pronounced as over land in all models. Over the maritime continent, most models have recreated the two-peak shape of the diurnal cycle. In the North Pacific region, the lack of a clear diurnal cycle, together with low TIWP values altogether was mostly successfully modelled. However, in contrast to other regions, models showed higher absolute TIWP than CCIC.

The individual models differ substantially in their diurnal cycle estimates. However, this is not easily attributed to specific model characteristics. These models not only differ in resolution, parameterisation and microphysics, but also in the inherent way that they were designed. An insightful comparison can only be possible if one aspect of the model is evaluated, with all the other characteristics remaining constant. For example, Atlas et al., 2024 compared four different microphysics schemes of varying complexity with the Global System for Atmospheric Modelling (GSAM) using an identical set-up. This resulted in considerably different TIWP distribution, with the version used in this thesis having the lowest TIWP estimates. Even at these high resolutions, the DYAMOND models still incorporate parameterisations for various processes such as the boundary layer, microphysics and cloudiness. Some models even included parameterisation for shallow convection (IFS, GFDL), which was still not a deciding factor regarding their performance. They have different radiation schemes, land surface models and initialisation strategies which trigger and modulate convection at different times. This makes interpreting their varied performances complex and outside the scope of this thesis.

Nevertheless, these models are still a considerable step forward when compared to GCMs. As an example, three GCMs have shown problems in reproducing the diurnal cycles of upper tropospheric IWP, reported in Eriksson et al., 2014. Interestingly, the performance was worse for South America than in Africa (in terms of whether there is an afternoon peak over tropical land or not). This is also something we observed here, for ERA5.

### 4.3.2 Global diurnal amplitude and peak time

DYAMOND average is compared with CCIC on a local level in Fig. 4.15. The amplitude and peak time for individual models are shown in Appendix A.4. The period was extended from 2018 to 2023 in CCIC. In relative terms, DYAMOND models reproduce the spatial patterns of amplitude very well. Amplitudes over the Indian subcontinent, inland Southeast Asia and the Tibetan plateau are slightly higher. In terms of peak time, both datasets show similar results over tropical land, with some smaller regional differences. In NH (Northern Hemisphere) land results for DYAMOND appear more noisy compared to the clear afternoon peak in CCIC. Early morning peak in tropical Indian and Atlantic oceans, and an afternoon peak in the extratropics can be seen on both, though there are some differences over the Pacific. Still, in regions where a strong diurnal cycle exists, the models and CCIC agree very well. Fig. 4.16 confirms the 24-hour component is the dominant mode of the DYAMOND diurnal cycle. Variance explained for the full fit can be seen in Appendix A.3.

Overall, we can say that the GSRMs in the DYAMOND project model the diurnal cycle of TIWP quite well. Being able to capture convective processes explicitly seems to be key to the right diurnal timing of TIWP.

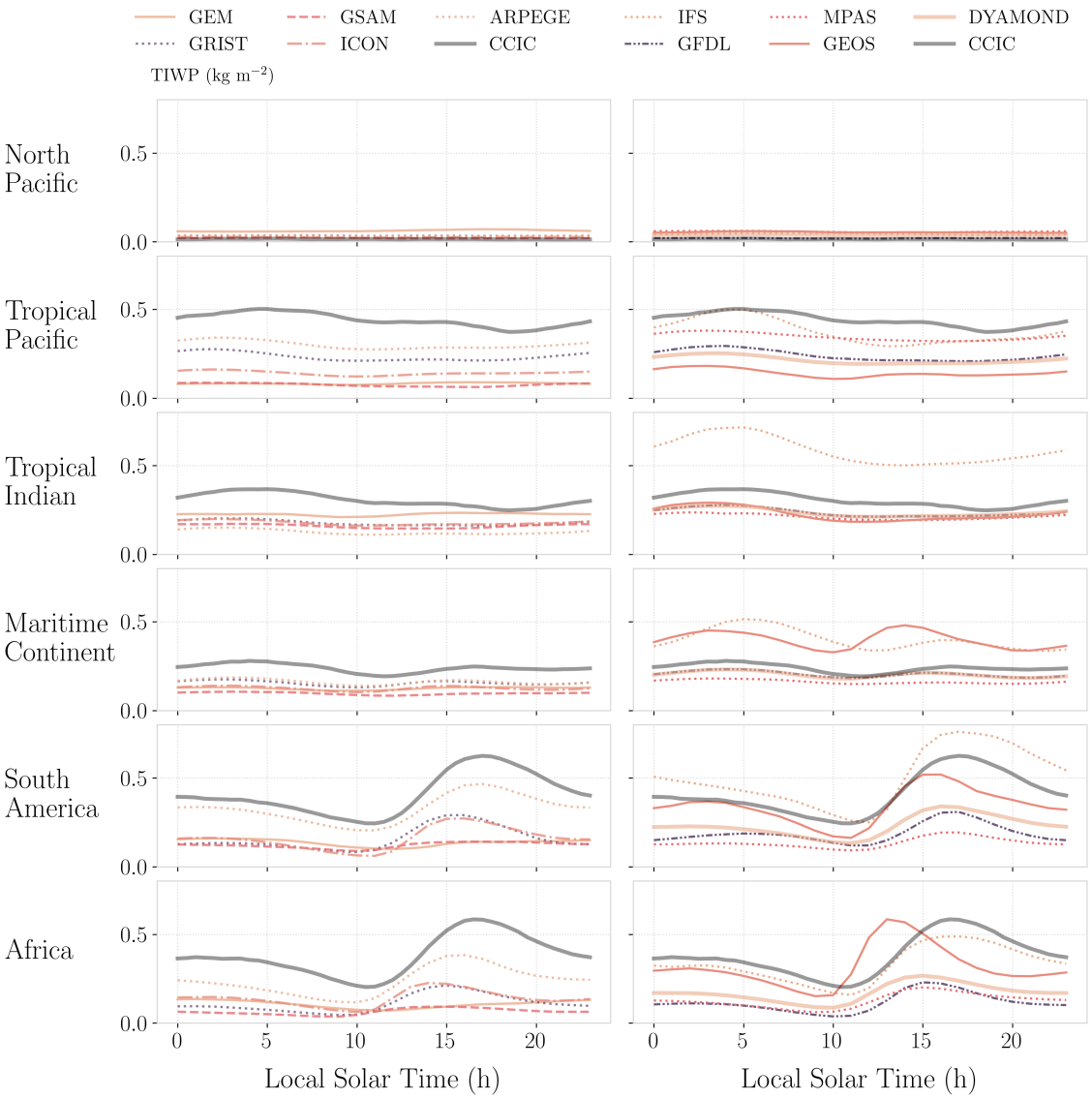


**Figure 4.13:** Mean regional diurnal cycles of TIWP for each DYAMOND model, for DYAMOND average and CCIC for February 2020. Two columns present different models, the one on the left including models with no convection parameterisation. They compare to the same CCIC data depicted with a thicker gray line.

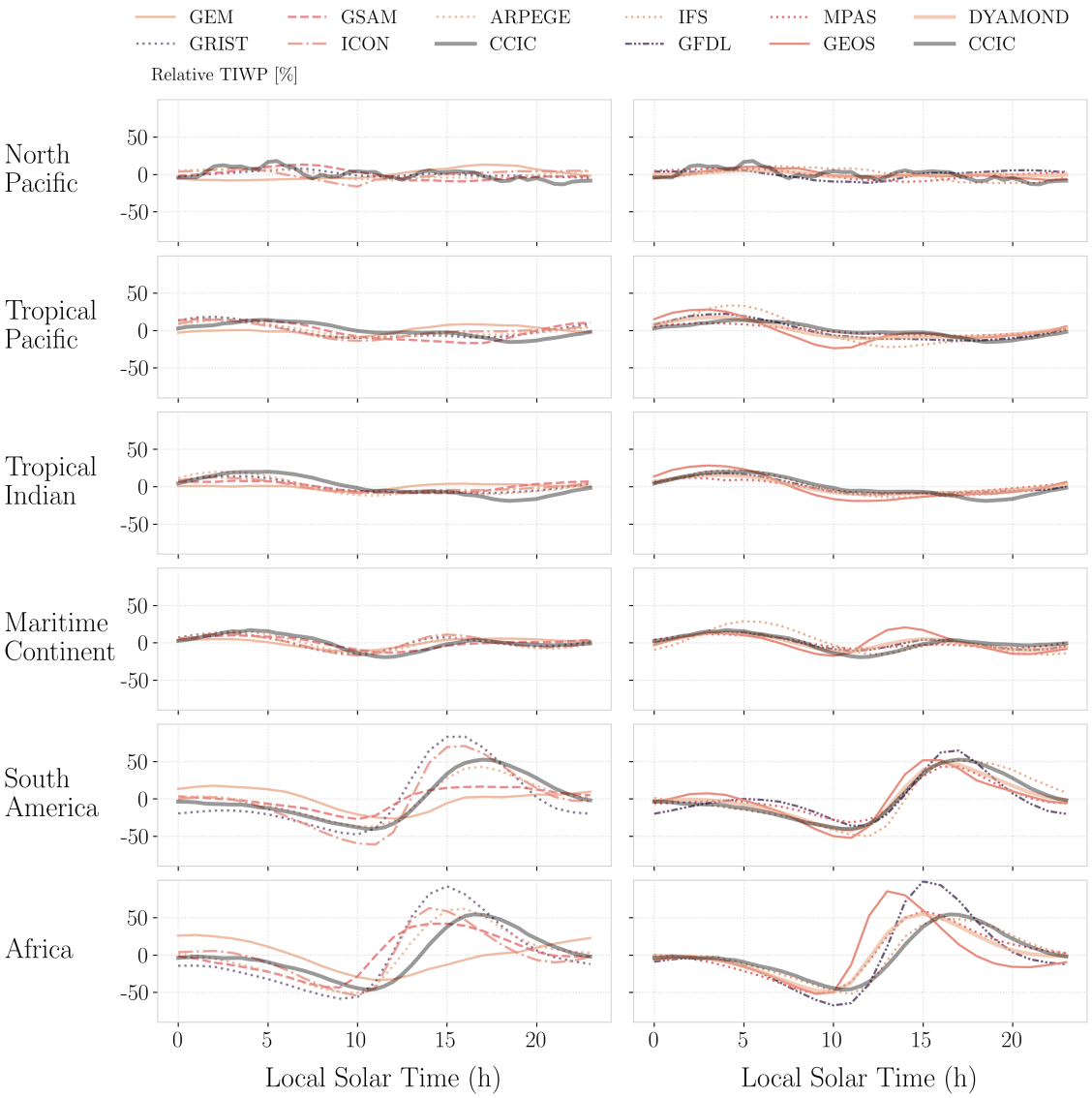


**Figure 4.14:** Deviation from mean TIWP [%] in regional diurnal cycles for each DYAMOND model and CCIC for February 2020. Two columns present different models, but compare to the same CCIC data depicted with a thicker gray line.

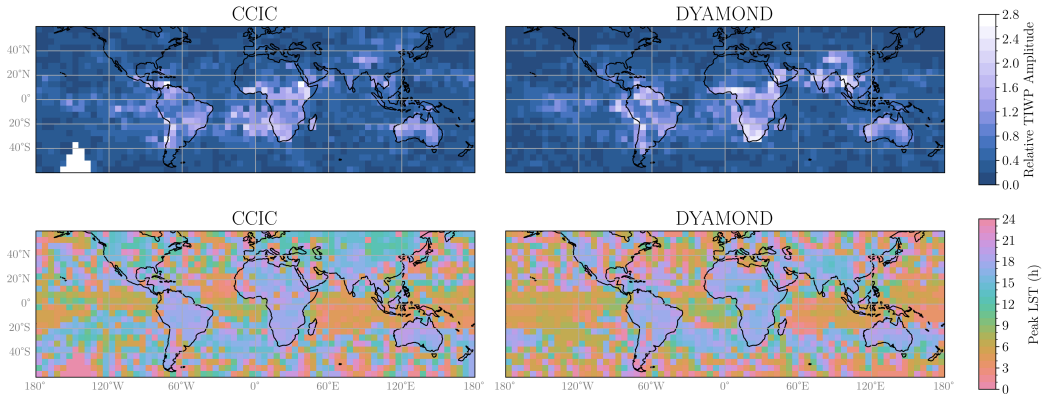


**Figure 4.15:** Diurnal amplitude (top) and peak time (bottom) after a harmonic fit, for February from 2018 to 2023 in CCIC (left) and for February 2020 in DYAMOND average (right) at a 5°x5° resolution. Amplitude is defined as the daily maximum minus the daily minimum divided by the local mean.

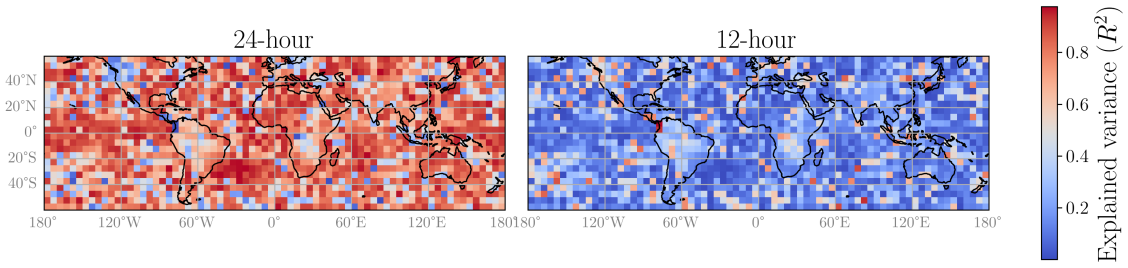


**Figure 4.16:** DYAMOND average explained variance ($R^2$) of the diurnal cycle by the 24-hour component (a) and 12-hour component (b) at each 5°x5° grid cell, for the years 2018 to 2023.

# 5

# Summary and conclusions

The diurnal cycle of cloud ice determines whether their radiative effect will be that of net cooling or net warming. This thesis provides the first semi-global diurnal analysis of the total ice water path (TIWP), thanks to the Chalmers Cloud Ice Climatology (CCIC). Using this record, we were able to evaluate ERA5 and GSRMs diurnal representations.

The key message is that ice clouds have a clear daily cycle that's fundamentaly different over land or ocean. Over land, particularly in tropical deep convective zones such as the Congo Basin, Amazon, and Maritime Continent, the diurnal signal is strong and peaks consistently in the afternoon, in agreement with solar-driven heating cycle of land. Orographic features and land-sea contrast have an important role in specific regions. TIWP diurnal cycle is more pronounced in the warmer season. The 24-hour harmonic mode is the primary driver of the TIWP diurnal cycle and the 12-hour component is only important to the extent that it improves the fit. Oceans show a more muted cycle peaking in the early morning in the tropics, and afternoon in the subtropics, driven by more complex processes.

Comparison with the ERA5 reanalysis reveals that while ERA5 captures some large-scale spatial and seasonal features of the diurnal cycle, it struggles to represents the phase and amplitude of the cycle, compared to CCIC. Further comparison with nine global convection-permitting models (CPMs) from the DYAMOND project showed that these models generally reproduce the diurnal cycle more realistically. They showed a clear capacity to simulate afternoon land peaks and early morning ocean peaks, though with a slight systematic tendency toward earlier peak times. This is still a substantial improvement compared to GCMs.

Despite the insights provided by this study, several limitations should be acknowledged. The main limitation is connected to the reference dataset itself, as CCIC contains biases inherited from its training dataset, 2C-ICE, which was reported to have 20 % higher estimates than DARDAR. While CCIC was the most suited record for our analysis, these limitations should be kept in mind. The CCIC dataset contains some missing data in the earlier years, because it was missing in the IR record used for input. Furthermore, to remove local spikes in the signal, the analysis applied 5°x5° spatial averaging, which may have smoothed out small-scale but meaningful regional features—especially over coastlines, mountain ranges, or islands. These results could be used to identify regions where the diurnal cycle could be further

investigated, perhaps at finer scales, in regions with a well defined diurnal cycle. Moreover, the study identified differences in the diurnal cycle between DYAMOND models but did not attempt to interpret them, which is beyond the scope of this thesis. Lastly, while there were no TIWP diurnal observations to compare to, these results could have been compared to the diurnal cycles of other observations such as lightning or precipitation data.

Future improvements could include comparing the CCIC record to precipitation and lightning diurnal cycles. Additionaly, since the CCIC record covers a long span of years, it would be interesting to see if climate change has impacted the TIWP diurnal cycle in any way.

Despite these limitations, this study demonstrated the value of the CCIC dataset in resolving the diurnal cycle of TIWP and validating climate models on the diurnal level. It was shown that the new storm resolving models show a clear step forward in reproducing these patterns, especially the land-ocean timing contrast. Ice clouds are a small part of the atmosphere, yet they have a disproportionate impact on the Earth's climate system. The prevailing albedo or greenhouse effect in deep tropical clouds is directly influenced by their diurnal cycle. Representing the daily variation more realistically is important for making accurate climate predictions.

# Bibliography


Amell, A., Pfreundschuh, S., & Eriksson, P. (2024). The Chalmers Cloud Ice Climatology: Retrieval implementation and validation. *Atmospheric Measurement Techniques*, *17*(14), 4337–4368. https://doi.org/10.5194/amt-17-4337-2024

Atlas, R. L., Bretherton, C. S., Sokol, A. B., Blossey, P. N., & Khairoutdinov, M. F. (2024). Tropical Cirrus Are Highly Sensitive to Ice Microphysics Within a Nudged Global Storm-Resolving Model. *Geophysical Research Letters*, *51*(1), e2023GL105868. https://doi.org/10.1029/2023GL105868

Bellenger, H., Takayabu, Y. N., Ushiyama, T., & Yoneyama, K. (2010). Role of Diurnal Warm Layers in the Diurnal Cycle of Convection over the Tropical Indian Ocean during MISMO. https://doi.org/10.1175/2010MWR3249.1

Bony, S., Stevens, B., Frierson, D. M. W., Jakob, C., Kageyama, M., Pincus, R., Shepherd, T. G., Sherwood, S. C., Siebesma, A. P., Sobel, A. H., Watanabe, M., & Webb, M. J. (2015). Clouds, circulation and climate sensitivity. *Nature Geoscience*, *8*(4), 261–268. https://doi.org/10.1038/ngeo2398

Businger, S., Graziano, T. M., Kaplan, M. L., & Rozumalski, R. A. (2005). Cold-air cyclogenesis along the Gulf-Stream front: Investigation of diabatic impacts on cyclone development, frontal structure, and track. *Meteorology and Atmospheric Physics*, *88*(1), 65–90. https://doi.org/10.1007/s00703-003-0050-y

Christopoulos, C., & Schneider, T. (2021). Assessing Biases and Climate Implications of the Diurnal Precipitation Cycle in Climate Models. *Geophysical Research Letters*, *48*(13), e2021GL093017. https://doi.org/10.1029/2021GL093017

Dai, A. (2001). Global Precipitation and Thunderstorm Frequencies. Part II: Diurnal Variations. Retrieved April 23, 2025, from https://journals.ametsoc.org/view/journals/clim/14/6/1520-0442_2001_014_1112_gpatfp_2.0.co_2.xml

Dai, A. (2024). The diurnal cycle from observations and ERA5 in precipitation, clouds, boundary layer height, buoyancy, and surface fluxes. *Climate Dynamics*, *62*(7), 5879–5908. https://doi.org/10.1007/s00382-024-07182-6

Dou, T., Xiao, C., Huang, Y., Yue, H., & Han, W. (2020). Estimation of the Atmospheric Ice Content Mass, Spatial Distribution, and Long-Term Changes Based on the ERA5 Reanalysis. *Geophysical Research Letters*, *47*(15), e2020GL088186. https://doi.org/10.1029/2020GL088186

Duncan, D. I., & Eriksson, P. (2018). An update on global atmospheric ice estimates from satellite observations and reanalyses. *Atmospheric Chemistry and Physics*, *18*(15), 11205–11219. https://doi.org/10.5194/acp-18-11205-2018

Eriksson, P., Rydberg, B., Johnston, M., Murtagh, D. P., Struthers, H., Ferrachat, S., & Lohmann, U. (2010). Diurnal variations of humidity and ice water content in the tropical upper troposphere. *Atmospheric Chemistry and Physics*, *10*(23), 11519–11533. https://doi.org/10.5194/acp-10-11519-2010

Eriksson, P., Rydberg, B., Sagawa, H., Johnston, M. S., & Kasai, Y. (2014). Overview and sample applications of SMILES and Odin-SMR retrievals of upper tropospheric humidity and cloud ice mass. *Atmospheric Chemistry and Physics*, *14*(23), 12613–12629. https://doi.org/10.5194/acp-14-12613-2014

Fedorov, A. V. (2007). Ocean-Atmosphere Coupling.

Gong, J., Zeng, X., Wu, D. L., & Li, X. (2018). Diurnal Variation of Tropical Ice Cloud Microphysics: Evidence from Global Precipitation Measurement Microwave Imager Polarimetric Measurements. *Geophysical Research Letters*, *45*(2), 1185–1193. https://doi.org/10.1002/2017GL075519

Hersbach, H., Bell, B., Berrisford, P., Hirahara, S., Horányi, A., Muñoz-Sabater, J., Nicolas, J., Peubey, C., Radu, R., Schepers, D., Simmons, A., Soci, C., Abdalla, S., Abellan, X., Balsamo, G., Bechtold, P., Biavati, G., Bidlot, J., Bonavita, M., … Thépaut, J.-N. (2020). The ERA5 global reanalysis. *Quarterly Journal of the Royal Meteorological Society*, *146*(730), 1999–2049. https://doi.org/10.1002/qj.3803

Hong, G., Heygster, G., & Rodriguez, C. A. M. (2006). Effect of cirrus clouds on the diurnal cycle of tropical deep convective clouds. *Journal of Geophysical Research: Atmospheres*, *111*(D6). https://doi.org/10.1029/2005JD006208

Illingworth, A. J., Barker, H. W., Beljaars, A., Ceccaldi, M., Chepfer, H., Clerbaux, N., Cole, J., Delanoë, J., Domenech, C., Donovan, D. P., Fukuda, S., Hirakata, M., Hogan, R. J., Huenerbein, A., Kollias, P., Kubota, T., Nakajima, T., Nakajima, T. Y., Nishizawa, T., … Zadelhoff, G.-J. v. (2015). The EarthCARE Satellite: The Next Step Forward in Global Measurements of Clouds, Aerosols, Precipitation, and Radiation. https://doi.org/10.1175/BAMS-D-12-00227.1

Intergovernmental Panel on Climate Change (IPCC). (2023). *Climate Change 2021 – The Physical Science Basis: Working Group I Contribution to the Sixth Assessment Report of the Intergovernmental Panel on Climate Change*. Cambridge University Press. https://doi.org/10.1017/9781009157896

Janowiak, J., Joyce, B., & Pingping, X. (2017). NCEP/CPC L3 Half Hourly 4km Global (60S - 60N) Merged IR V1. https://doi.org/10.5067/P4HZB9N27EKU

Jeong, J.-H., Walther, A., Nikulin, G., Chen, D., & Jones, C. (2011). Diurnal cycle of precipitation amount and frequency in Sweden: Observation versus model simulation. *Tellus A: Dynamic Meteorology and Oceanography*, *63*(4). Retrieved June 6, 2025, from https://a.tellusjournals.se/articles/10.1111/j.1600-0870.2011.00517.x

Jiang, J. H., Su, H., Zhai, C., Shen, T. J., Wu, T., Zhang, J., Cole, J. N. S., Salzen, K. v., Donner, L. J., Seman, C., Genio, A. D., Nazarenko, L. S., Dufresne, J.-L., Watanabe, M., Morcrette, C., Koshiro, T., Kawai, H., Gettelman, A., Millán, L., … Shiotani, M. (2015). Evaluating the Diurnal Cycle of Upper-

Tropospheric Ice Clouds in Climate Models Using SMILES Observations. https://doi.org/10.1175/JAS-D-14-0124.1

Johnson, R. H., Rickenbach, T. M., Rutledge, S. A., Ciesielski, P. E., & Schubert, W. H. (1999). Trimodal Characteristics of Tropical Convection. Retrieved April 13, 2025, from https://journals.ametsoc.org/view/journals/clim/12/8/1520-0442_1999_012_2397_tcotc_2.0.co_2.xml

Kikuchi, K.-i., Nishibori, T., Ochiai, S., Ozeki, H., Irimajiri, Y., Kasai, Y., Koike, M., Manabe, T., Mizukoshi, K., Murayama, Y., Nagahama, T., Sano, T., Sato, R., Seta, M., Takahashi, C., Takayanagi, M., Masuko, H., Inatani, J., Suzuki, M., & Shiotani, M. (2010). Overview and early results of the Superconducting Submillimeter-Wave Limb-Emission Sounder (SMILES). *Journal of Geophysical Research: Atmospheres*, *115*(D23). https://doi.org/10.1029/2010JD014379

Lai, H.-W., Ou, T., Dai, A., Chen, X., & Chen, A. (2025). Diurnal Cycle of Summer Precipitation Over Mainland Southeast Asia Revealed by Observations, Reanalysis, and Dynamic Downscaling. *Journal of Geophysical Research: Atmospheres*, *130*(11), e2024JD043020. https://doi.org/10.1029/2024JD043020

Lohmann, U., Lüönd, F., & Mahrt, F. (2016). *An Introduction to Clouds: From the Microscale to Climate*. Cambridge University Press. https://doi.org/10.1017/CBO9781139087513

Millán, L., Read, W., Kasai, Y., Lambert, A., Livesey, N., Mendrok, J., Sagawa, H., Sano, T., Shiotani, M., & Wu, D. L. (2013). SMILES ice cloud products. *Journal of Geophysical Research: Atmospheres*, *118*(12), 6468–6477. https://doi.org/10.1002/jgrd.50322

Pfreundschuh, S., Kukulies, J., Amell, A., Hallborn, H., May, E., & Eriksson, P. (2025). The Chalmers Cloud Ice Climatology: A Novel Robust Climate Record of Frozen Cloud Hydrometeor Concentrations. *Journal of Geophysical Research: Atmospheres*, *130*(6), e2024JD042618. https://doi.org/10.1029/2024JD042618

Roh, W., Satoh, M., & Hohenegger, C. (2021). Intercomparison of Cloud Properties in DYAMOND Simulations over the Atlantic Ocean. *Journal of the Meteorological Society of Japan. Ser. II*, *99*(6), 1439–1451. https://doi.org/10.2151/jmsj.2021-070

Schulzweida, U. (2023). CDO User Guide. https://doi.org/10.5281/zenodo.10020800

Song, J., Song, F., Feng, Z., Leung, L. R., Li, C., & Wu, L. (2024). Realistic Precipitation Diurnal Cycle in Global Convection-Permitting Models by Resolving Mesoscale Convective Systems. *Geophysical Research Letters*, *51*(13), e2024GL109945. https://doi.org/10.1029/2024GL109945

Stensrud, D. J. (2007, May). *Parameterization Schemes: Keys to Understanding Numerical Weather Prediction Models*. Cambridge University Press.

Stephens, G. L., Vane, D. G., Boain, R. J., Mace, G. G., Sassen, K., Wang, Z., Illingworth, A. J., O'connor, E. J., Rossow, W. B., Durden, S. L., Miller, S. D., Austin, R. T., Benedetti, A., & Mitrescu, C. (2002). THE CLOUDSAT MISSION AND THE A-TRAIN. https://doi.org/10.1175/BAMS-83-12-1771

Stevens, B., Satoh, M., Auger, L., Biercamp, J., Bretherton, C. S., Chen, X., Düben, P., Judt, F., Khairoutdinov, M., Klocke, D., Kodama, C., Kornblueh, L., Lin,

S.-J., Neumann, P., Putman, W. M., Röber, N., Shibuya, R., Vanniere, B., Vidale, P. L., ... Zhou, L. (2019). DYAMOND: The DYnamics of the Atmospheric general circulation Modeled On Non-hydrostatic Domains. *Progress in Earth and Planetary Science*, *6*(1), 61. https://doi.org/10.1186/s40645-019-0304-z

Sui, C.-H., Lau, K.-M., Takayabu, Y. N., & Short, D. A. (1997). Diurnal Variations in Tropical Oceanic Cumulus Convection during TOGA COARE. Retrieved April 23, 2025, from https://journals.ametsoc.org/view/journals/atsc/54/5/1520-0469_1997_054_0639_dvitoc_2.0.co_2.xml

Tian, B., Soden, B. J., & Wu, X. (2004). Diurnal cycle of convection, clouds, and water vapor in the tropical upper troposphere: Satellites versus a general circulation model. *Journal of Geophysical Research: Atmospheres*, *109*(D10). https://doi.org/10.1029/2003JD004117

Waliser, D. E., Li, J.-L. F., Woods, C. P., Austin, R. T., Bacmeister, J., Chern, J., Del Genio, A., Jiang, J. H., Kuang, Z., Meng, H., Minnis, P., Platnick, S., Rossow, W. B., Stephens, G. L., Sun-Mack, S., Tao, W.-K., Tompkins, A. M., Vane, D. G., Walker, C., & Wu, D. (2009). Cloud ice: A climate model challenge with signs and expectations of progress. *Journal of Geophysical Research: Atmospheres*, *114*(D8). https://doi.org/10.1029/2008JD010015

Watters, D., & Battaglia, A. (2019). The Summertime Diurnal Cycle of Precipitation Derived from IMERG. *Remote Sensing*, *11*(15), 1781. https://doi.org/10.3390/rs11151781

Wedi, N., & Malardel, S. (2010). Non-hydrostatic modelling at ECMWF. https://doi.org/10.21957/RZOJR98E

Winker, D. M., Pelon, J., Coakley, J. A., Ackerman, S. A., Charlson, R. J., Colarco, P. R., Flamant, P., Fu, Q., Hoff, R. M., Kittaka, C., Kubar, T. L., Treut, H. L., Mccormick, M. P., Mégie, G., Poole, L., Powell, K., Trepte, C., Vaughan, M. A., & Wielicki, B. A. (2010). The CALIPSO Mission. https://doi.org/10.1175/2010BAMS3009.1

Yang, G.-Y., & Slingo, J. (2001). The Diurnal Cycle in the Tropics. Retrieved April 13, 2025, from https://journals.ametsoc.org/view/journals/mwre/129/4/1520-0493_2001_129_0784_tdcitt_2.0.co_2.xml

Zhao, Y., Li, J., Zhang, L., Deng, C., Li, Y., Jian, B., & Huang, J. (2023). Diurnal cycles of cloud cover and its vertical distribution over the Tibetan Plateau revealed by satellite observations, reanalysis datasets, and CMIP6 outputs. *Atmospheric Chemistry and Physics*, *23*(1), 743–769. https://doi.org/10.5194/acp-23-743-2023

# A

# Appendix

## A.1 Appendix 1

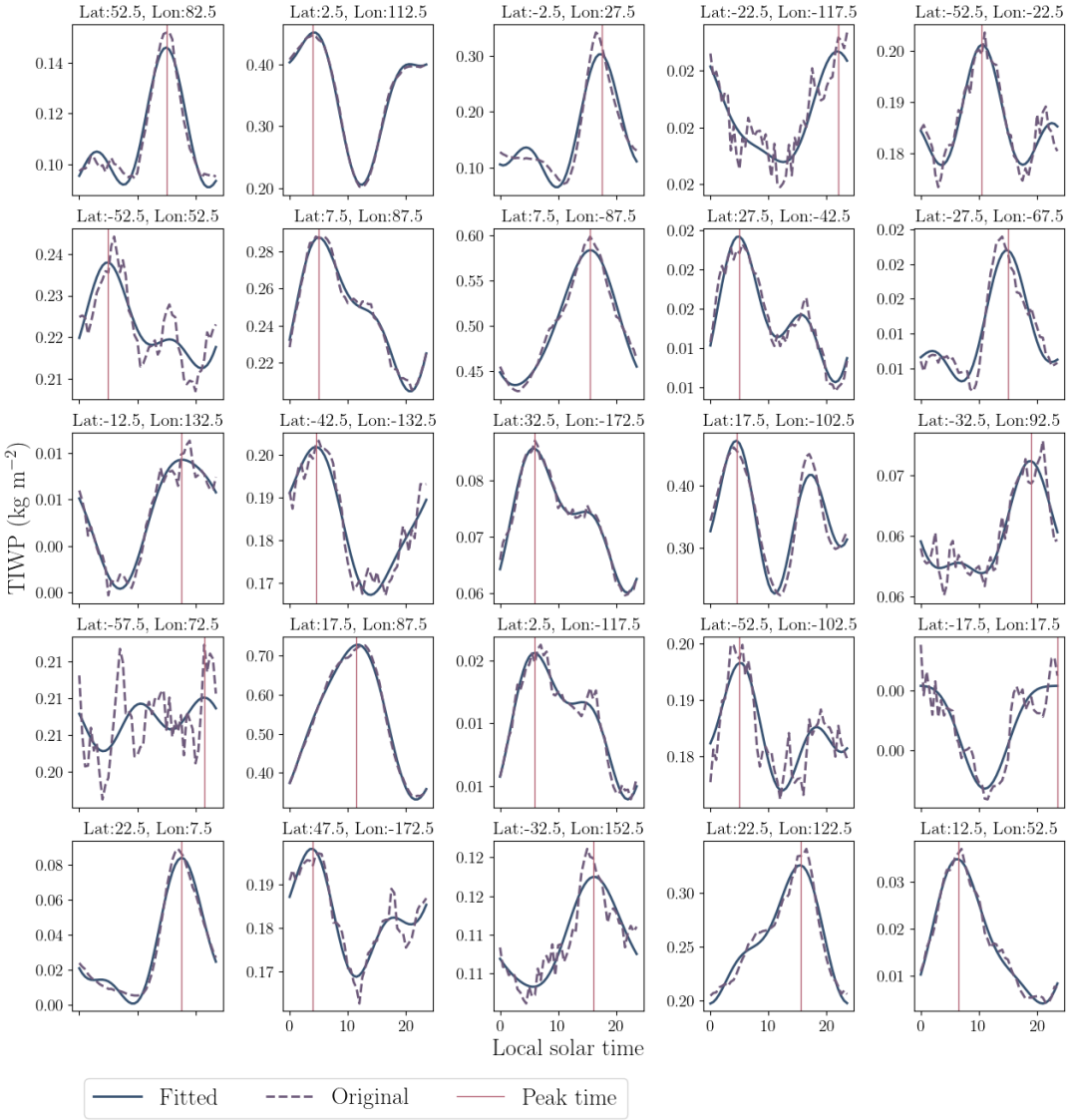


**Figure A.1:** Examples from 25 randomly selected grid cells for which harmonic fitting was performed. Results show CCIC data for JJA from 2018 to 2023.

## A.2 Appendix 2

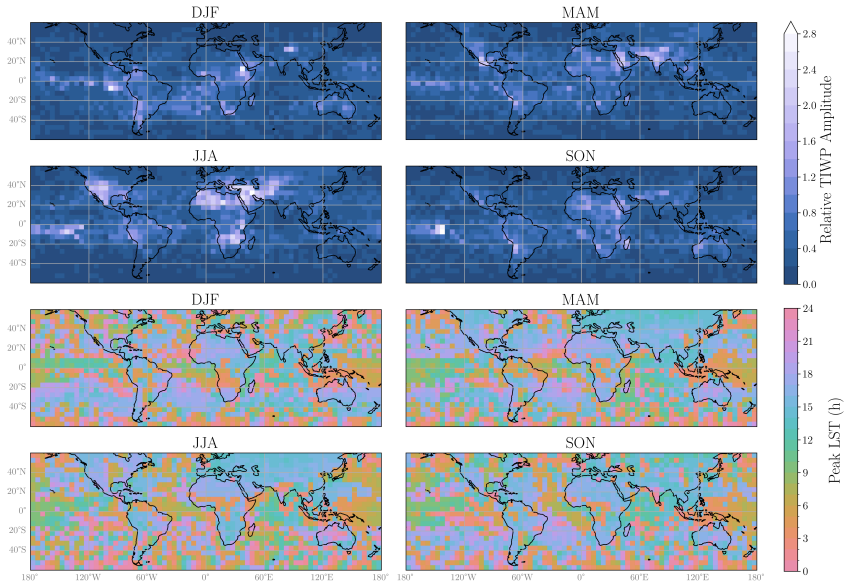


**Figure A.2:** ERA diurnal amplitude (top) and peak time (bottom) after a harmonic fit, for the years 2018 to 2023 at a 5°x5° resolution, for the four seasons.

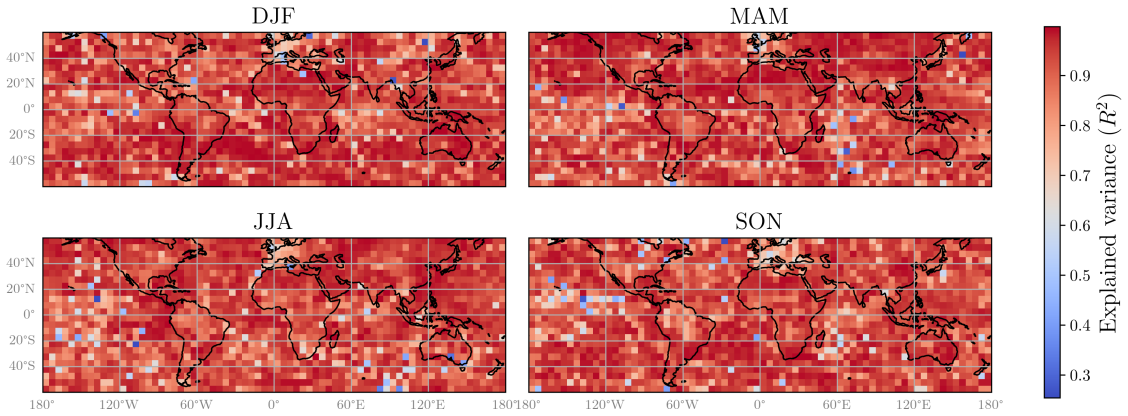


**Figure A.3:** ERA5 Explained variance ($R^2$) of the diurnal cycle by the harmonic fit at each 5°x5° grid cell, for the years 2018 to 2023.

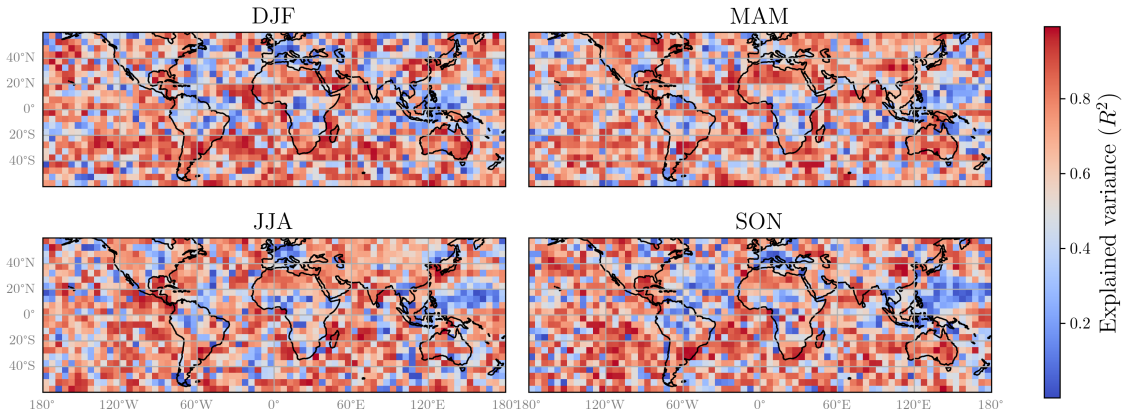


**Figure A.4:** ERA5 explained variance ($R^2$) of the diurnal cycle by the 24-hour component at each 5°x5° grid cell, for the years 2018 to 2023.

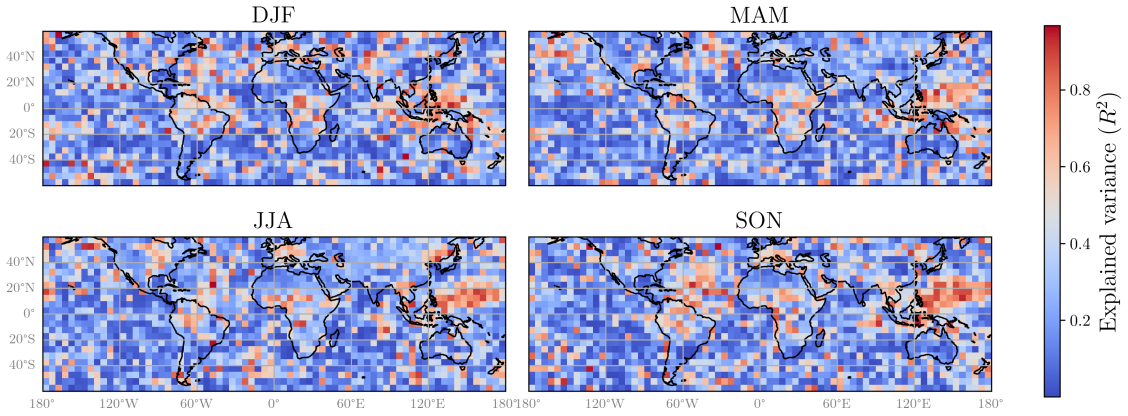


**Figure A.5:** ERA5 explained variance ($R^2$) of the diurnal cycle by the 12-hour component at each 5°x5° grid cell, for the years 2018 to 2023.

## A.3 Appendix 3

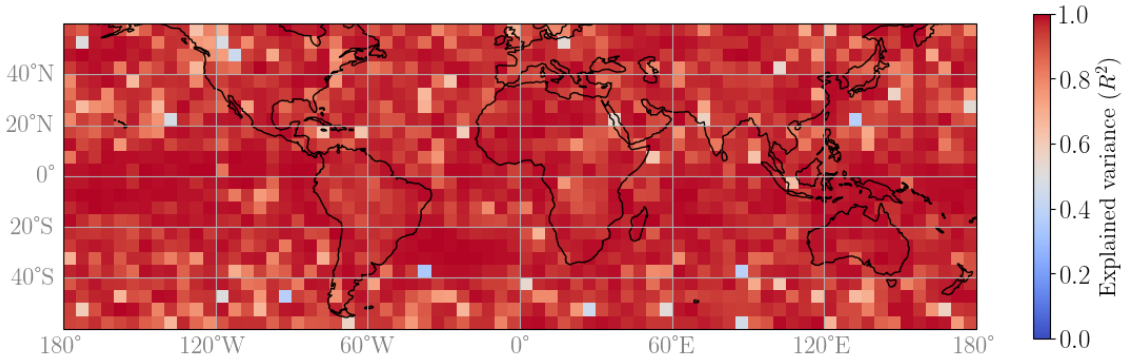


**Figure A.6:** DYAMOND average explained variance ($R^2$) of the diurnal cycle by the fitted diurnal cycle at each 5°x5° grid cell, for the years 2018 to 2023.

## A.4 Appendix 4

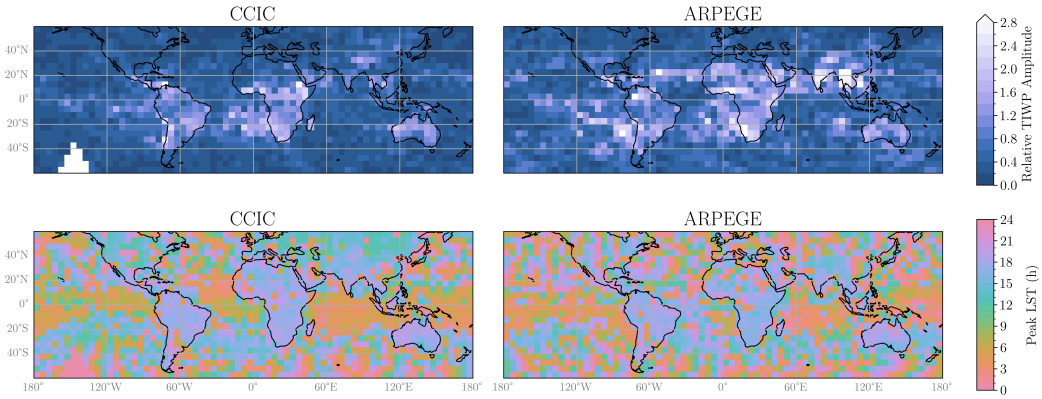


**Figure A.7:** Diurnal amplitude (top) and peak time (bottom) after a harmonic fit, for February from 2018 to 2023 in CCIC (left) and for February 2020 in ARPEGE (right) at a 5°x5° resolution. Amplitude is defined as the daily maximum minus the daily minimum divided by the local mean.

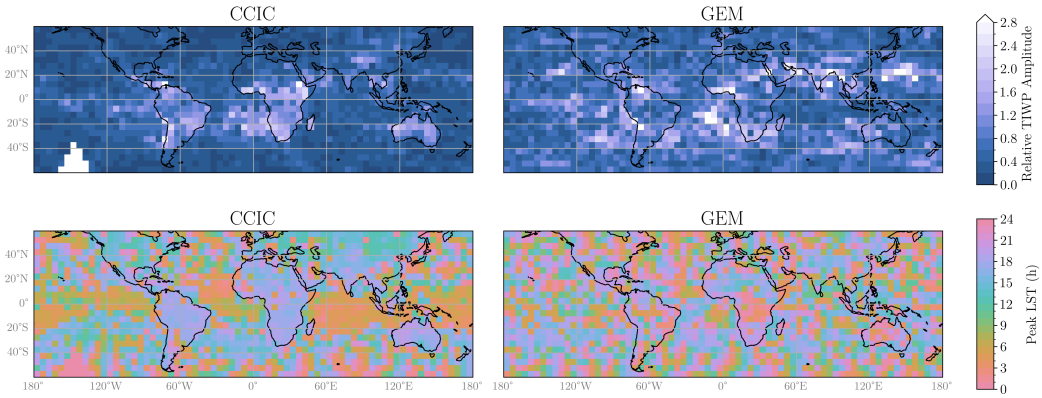


**Figure A.8:** Same as in Fig A.7, but for GEM.

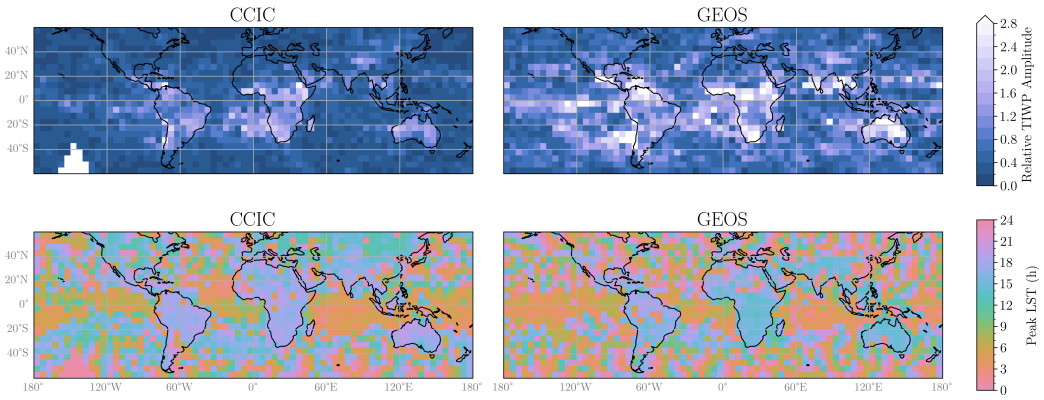


**Figure A.9:** Same as in Fig A.7, but for GEOS.

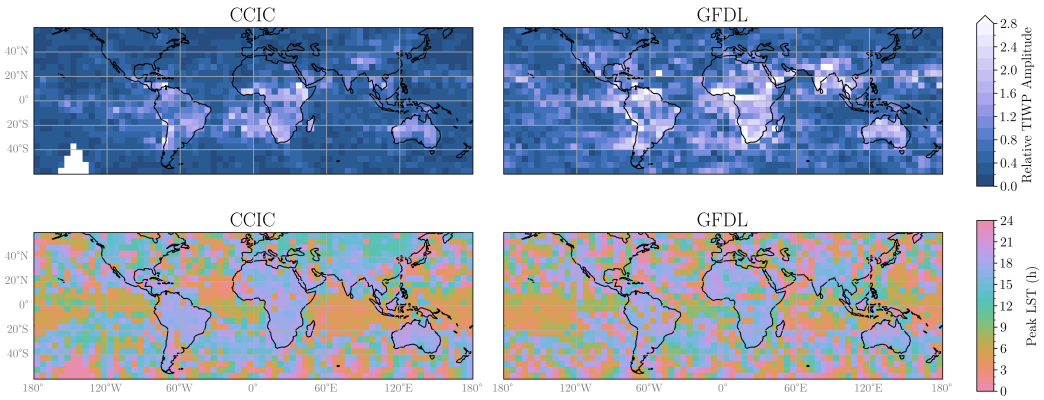


**Figure A.10:** Same as in Fig A.7, but for GFLD.

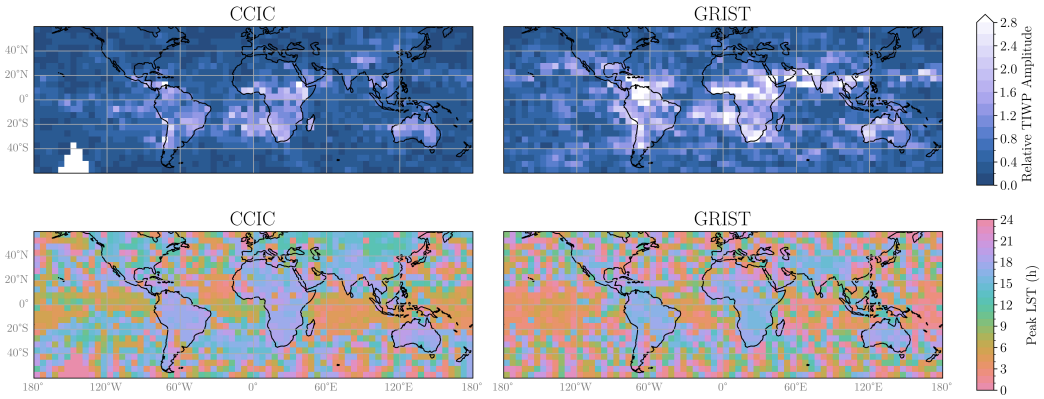


**Figure A.11:** Same as in Fig A.7, but for GRIST.

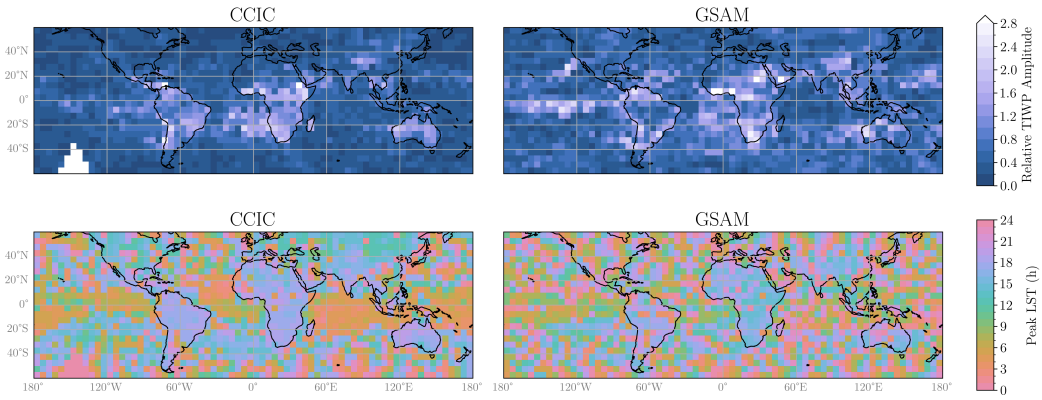


**Figure A.12:** Same as in Fig A.7, but for GSAM.

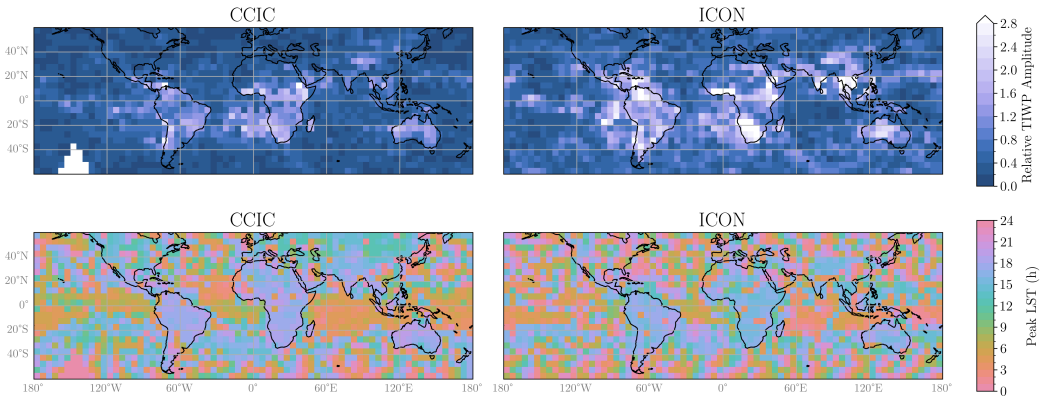


**Figure A.13:** Same as in Fig A.7, but for ICON.

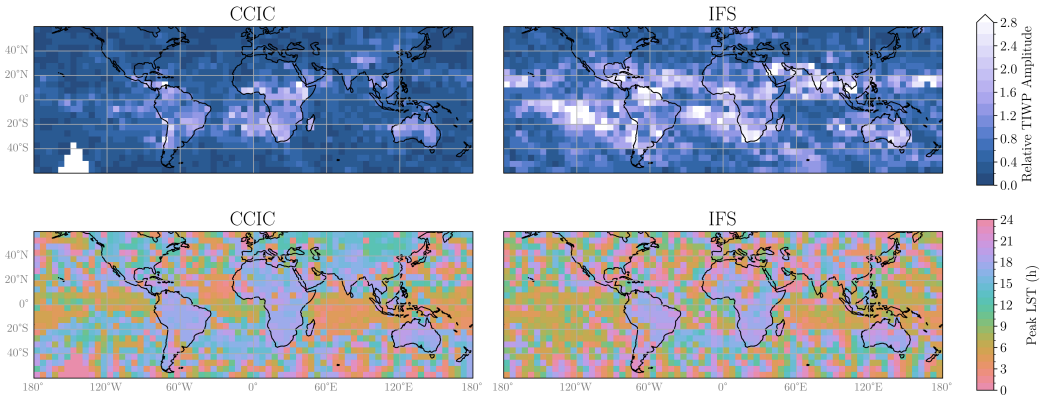


**Figure A.14:** Same as in Fig A.7, but for IFS.

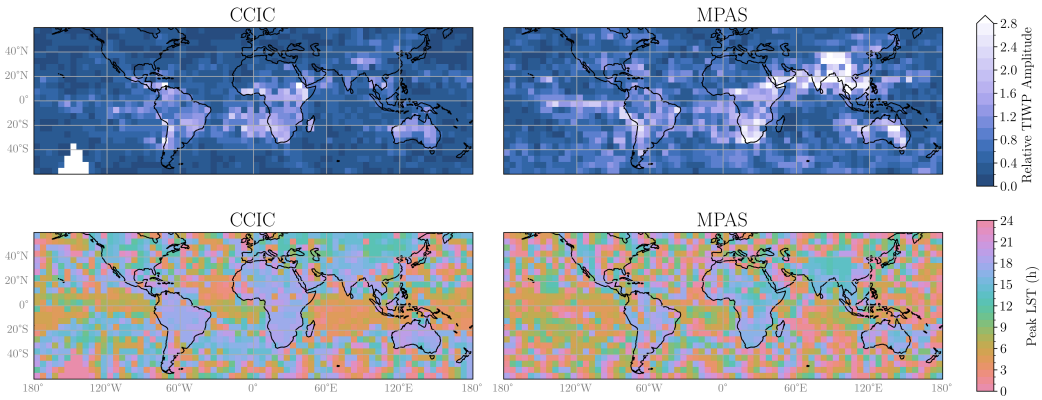


**Figure A.15:** Same as in Fig A.7, but for MPAS.